Photosystem II: The Reaction Center of Oxygenic Photosynthesis*

David J. Vinyard,[1,2] Gennady M. Ananyev,[1] and G. Charles Dismukes[1]

[1]Department of Chemistry and Chemical Biology and the Waksman Institute of Microbiology, Rutgers, The State University of New Jersey, Piscataway, New Jersey 08854; email: ananyev@rci.rutgers.edu, dismukes@rci.rutgers.edu

[2]Department of Chemistry, Princeton University, Princeton, New Jersey 08540; email: dvinyard@princeton.edu

Annu. Rev. Biochem. 2013. 82:577–606

First published online as a Review in Advance on March 18, 2013

The *Annual Review of Biochemistry* is online at biochem.annualreviews.org

This article's doi: 10.1146/annurev-biochem-070511-100425

*This article is dedicated to the memory of Professor Gernot Renger, pioneer in photosystem II research.

Keywords

oxygen evolution, photoassembly, photoprotection, proton-coupled electron transport, period-four oscillations, water oxidation kinetics, water oxidation thermodynamics

Abstract

Photosystem II (PSII) uses light energy to split water into chemical products that power the planet. The stripped protons contribute to a membrane electrochemical potential before combining with the stripped electrons to make chemical bonds and releasing O_2 for powering respiratory metabolisms. In this review, we provide an overview of the kinetics and thermodynamics of water oxidation that highlights the conserved performance of PSIIs across species. We discuss recent advances in our understanding of the site of water oxidation based upon the improved (1.9-Å resolution) atomic structure of the Mn_4CaO_5 water-oxidizing complex (WOC) within cyanobacterial PSII. We combine these insights with recent knowledge gained from studies of the biogenesis and assembly of the WOC (called photoassembly) to arrive at a proposed chemical mechanism for water oxidation.

Contents

WOC: water-oxidizing complex

PSII: photosystem II

Thylakoid membrane: lipid bilayer inside cyanobacteria and chloroplasts containing photosynthetic complexes (and respiratory complexes in cyanobacteria)

INTRODUCTION

Natural photosynthesis dominates the biosphere as the most widespread and successful metabolism on Earth (1). Among photosynthetic organisms, the oxygenic phototrophs are the most prolific, comprising all known species of cyanobacteria, algae, and higher plants. The early ancestors of these organisms transformed the surface of Earth beginning circa 3 billion years ago from a drab aluminosilicate composite to a lush green carpet visible from outer space. This transformation was powered by two highly successful metabolic innovations (2). First, the innovation of reaction center photochemistry and the water-oxidizing complex (WOC) in photosystem II (PSII) produced both redox energy, carried as O_2 and hydrogen in plastoquinol (PQH_2) (Equation 1*a*,*b*), and the proton motive force (*pmf* ~ ΔpH) across the thylakoid membrane. Later, the second innovation, respiration, combined the oxidation of hydrogen carriers with O_2 reduction, *pmf* formation, and ultimately energy storage in phosphate ester bonds:

$$2H_2O + 4h\nu \rightarrow 4e^- + O_2 + 4H^+_{lumen}, \quad 1a.$$

$$2PQ + 4e^- + 4H^+_{stroma} \rightarrow 2PQH_2. \quad 1b.$$

Remarkably, despite their enormous phylogenetic and ecological diversity, all contemporary oxygenic phototrophs characterized to date use an identical PSII inorganic core and conserved subunits for solar energy conversion. Stated differently, three billion years of evolution under the far-ranging biogeochemical forces since the accretion of Earth have produced only a single blueprint for catalyzing water-splitting chemistry. The evolution of a single enzymatic solution despite access to every ecological niche and the vast time period is exceedingly rare in biology! To learn from this lesson, we must understand the physicochemical principles by which PSII operates (3, 4). This is a main goal of this review. These principles can be applied to designing bioinspired water oxidation catalysts and bioengineering reaction centers (5, 6). The factors determining PSII solar energy conversion efficiency are described below (see PSII Reaction Center Efficiency). We begin here with a general introduction.

The net reaction of PSII (Equation 1) is enabled by chlorophyll (Chl), which both captures light and converts it into chemical energy. Five chemically distinct Chls have been identified in light-harvesting complexes of oxygenic phototrophs: Chls *a*, *b*, *c*, *d*, and *f* (7–9). Most PSII reaction centers utilize Chl *a* [λ_{max} = 665 nm in methanol (10)] for primary charge separation. However, the cyanobacterium *Acaryochloris marina* utilizes Chl *d*

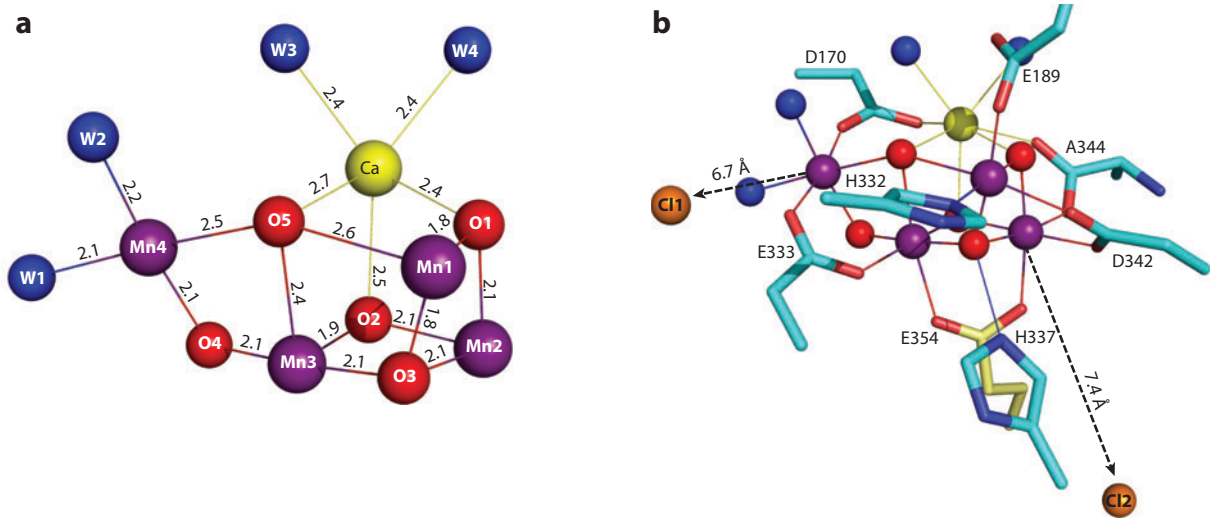

Figure 1

Structure of the photosystem II water-oxidizing complex (WOC) as revealed by the 1.9-Å resolution X-ray diffraction structure by Umena et al. (17). (*a*) The $Mn_4CaO_5(H_2O)_4$ core with bond distances in angstroms. (*b*) First coordination sphere ligand environment of the WOC core. Amino acid residues from the D1 subunit are shown in cyan, and those from the CP43 subunit are in yellow. The relative positions of the two chloride ions are also shown. Images generated in the PyMOL program using Protein Data Bank entry 3ARC (17).

[$\lambda_{max} = 697$ nm in methanol (11)] to split water. Chl *f* was recently found within a filamentous cyanobacterium derived from stromatolites and has the longest absorbance wavelength of all Chls at $\lambda_{max} = 707$ nm (in methanol) (11). Whether it too can replace Chl *a* in the PSII reaction center remains to be shown.

Turning to the PSII-WOC, the elemental composition, electronic coupling, and inter-manganese distances within the Mn_4CaO_x core have been established by reconstitution (12) and spectroscopic studies (reviewed in Reference 13). X-ray diffraction (XRD) studies of PSII core protein complexes have revealed the atomic coordinates of the metal-oxo cluster in its dark-stable state, $Mn_4CaO_5(H_2O)_4$ (**Figure 1**) (14–17). If cells are dark adapted and then subjected to a series of single-turnover flashes (STFs), the greatest yield of oxygen is released on the third flash and every fourth flash thereafter in a damped period-four pattern (**Figure 2*b***) (18). All modern proposals concerning the mechanism of water oxidation adopt the time-tested work of Kok and coworkers (19, 20), who interpreted the data of Joliot et al. (18) by proposing that oxygen is released upon the linear accumulation of four charges through a cycle of four intermediates or S states (Equation 2; **Figure 2*a***). Fourier transform (FT) analysis of the oscillations (**Figure 2*c***) provides the frequency components that contribute to damping the oscillations. A single frequency is typically obtained and provides a model-independent measure of the turnover probability through the catalytic cycle (the cycle period is also used and has a maximum theoretical value of four flashes):

$$S_0 \xrightarrow{h\nu} S_1^{+1} \xrightarrow{h\nu} S_2^{+2} \xrightarrow{h\nu} S_3^{+3} \xrightarrow{h\nu} S_4^{+4} \longrightarrow O_2 + S_0. \quad 2.$$

Several other spectroscopic markers also exhibit period-four oscillations, including the Chl *a* variable fluorescence emission from PSII (F_v, which is discussed in detail in Light to Chemical Conversion Efficiency in PSII, below) (21). When O_2 yield and F_v are monitored simultaneously, overlap of the FTs clearly shows that

Chl: chlorophyll

STF: single-turnover flash

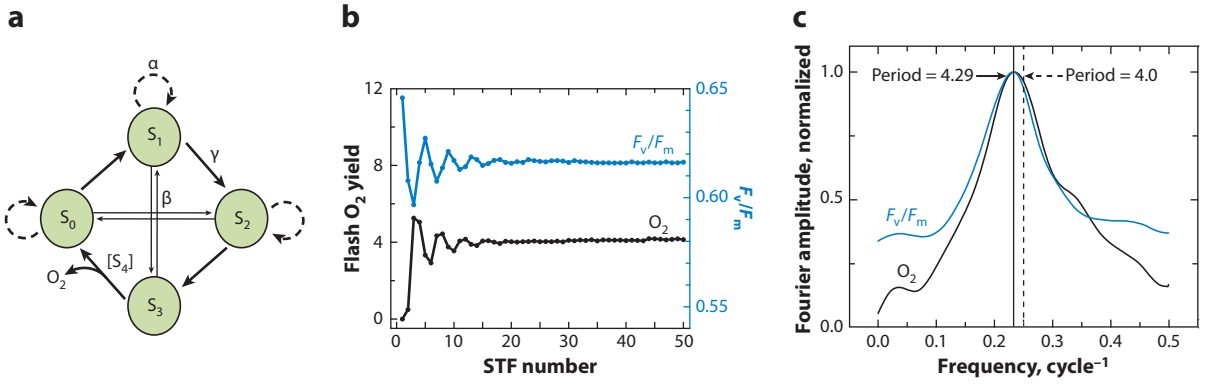

Figure 2

(*a*) The classic Kok model. Starting from the dark-stable S_1 state, a reaction center progresses to S_2 with probability γ (hit) following a single-turnover flash (STF). O_2 is released following the third flash through the S_4 intermediate, and the cycle resets to S_0. Damping of oscillations is accounted for by the inefficiency parameters [miss (α) and double hit (β)]. (*b*) Simultaneously measured oscillations in flash O_2 yield (*black*) and variable Chl-*a* fluorescence yield (F_v/F_m, *blue*) in *Arthrospira maxima* whole cells and (*c*) corresponding Fourier transforms. Based on raw data from Reference 21, in which 50 STFs were applied at 0.5 Hz following 5-min dark adaptation; the signal was averaged 40 times.

both methods are affected by the same physical process (**Figure 2**). Below (see Light to Chemical Conversion Efficiency in PSII), we discuss how this method has expanded our toolbox to allow measurement of the WOC turnover rate in vivo in many different oxygenic phototrophs.

STRUCTURE

Cellular Localization and Composition

PSII exists in vivo in the thylakoid membrane as a dimer, with each monomer containing 19–31 polypeptide subunits (length is species dependent and reviewed in References 22–24). Thylakoid membranes in the chloroplasts of higher plants are arranged in structured stacks (grana) and single sheets (lamella). Assembled PSII in plants is segregated from photosystem I (PSI), as it is preferentially localized in the grana as revealed by biochemistry (25) and electron microscopy studies (26, 27). The chloroplasts of algae typically do not have the elegantly defined grana stacks of higher plants, and less is known about the exact localization of PSII, although isolated appressed thylakoids are enriched in PSII relative to bulk thylakoids (28). The content of PSII in thylakoids relative to PSI and antenna complexes varies with organism, light intensity, and spectral wavelength in a manner reflecting the need for reductant versus the need for *pmf* and ATP (29).

In cyanobacteria, PSII is found throughout the thylakoid membrane system within the singular cellular compartment. Only in the primitive cyanobacterium *Gloeobacter violaceus* is PSII localized to the cytoplasmic membrane owing to an unusual absence of thylakoid membranes (30).

At least three extrinsic (soluble) subunits are associated with the lumenal side of PSII in green algae and higher plants: PsbO (33 kDa, also known as the Mn-stabilizing protein), PsbP (23 kDa), and PspQ (16 kDa). These subunits protect the inorganic core of the WOC and may play a role in proton evolution (for recent reviews, see References 31, 32). Interestingly, the extrinsic (lumenal) subunits of cyanobacterial PSII differ from those found in green algae and higher plants. PsbO is conserved, but PsbP and PsbQ are replaced with homologs CyanoP and CyanoQ. In addition, cyanobacterial PSII contains the soluble subunits PsbU (12 kDa) and PsbV (cyt c_{550}), which are not found in green algae and higher plants (31, 32). Although the binding of cyt c_{550} enhances PSII activity by

promoting the binding of PsbO, PsbU, Ca^{2+}, and Cl^{-} (33–38), a precise role for the redox-active heme group is unclear (reviewed in Reference 39). The red algae (Rhodophyta) and brown algae (Bacillariophyta or diatoms) also contain PsbU and PsbV in addition to PsbO, PsbP, and a homolog of PsbQ, PsbQ′ (31).

The Reaction Center

Whereas the low-molecular-weight and extrinsic subunits of PSII vary among diverse oxygenic phototrophs, the reaction center (RC) core is remarkably conserved. The RC core is defined as the minimal set of subunits required to oxidize water and has been experimentally determined to include D1, D2, CP43, CP47, and cyt b_{559} (α- and β-subunits). The only significant variation observed to date in core proteins is in the D1 subunit of cyanobacteria. At least four classes of D1 isoforms have been identified in cyanobacteria (40). The expression of these protein isoforms is controlled by differential transcriptional regulation of multiple *psbA* gene copies within a single genome (40, 41). Subtle differences in the amino acid sequences of these D1 isoforms control the efficiency of PSII specifically at very high and very low light intensities (42–45) or under low-oxygen conditions (46, 47). By contrast, green algae and plants contain only a single D1 isoform (40) and consequently utilize a different regulation system for dealing with varying light intensities.

The Water-Oxidizing Complex

The structure of the inorganic cluster where water is oxidized has been the subject of significant study for decades, and extensive knowledge has accumulated from spectroscopic and other sources. In 2011, the 1.9-Å XRD structure of PSII from *Thermosynechococcus vulcanus* by Umena et al. (17) provided a significantly higher-resolution map at the atomic level of the PSII-WOC in its dark-stable S_1 state (**Figure 1**). This structure was built upon earlier XRD reports of a closely related cyanobacterial PSII-WOC that first established many of the structural insights (14–16).

The WOC core is composed of an irregular cubical cluster or heterocubane, $CaMn_3O_4$ [as established by Ferreira et al. (15)], bridged by corner Mn3 to Mn4 (exocuboidal) via chemically distinct μ-oxos (μ_2-O4 and μ_4-O5; see **Figure 1*a*** for numbering) differing in their coordination and bonding types. At first glance, the ligand coordination numbers are normal, six for each Mn atom and seven for Ca (**Figure 1*b***). However, Mn1, Mn3, Mn4, and Ca have exceptionally long distances to corner μ_4-O5 (2.4–2.7 Å), which are longer than typical covalent bond lengths for these atom types and therefore form considerably weaker bonds. The consequences of these weak interactions and this unusual geometry are discussed in the following sections.

Oxygen atoms O1, O2, and O3 are the remaining corner oxos within the Mn_3CaO_4 heterocubane, and each is bonded to three metals. Each of these oxos is more weakly bonded (hydrogen bonded) to a fourth ligand (W923, CP43-R357, and D1-H337, respectively) (17), yielding four-coordinate oxos (μ_4-oxos) in distorted tetrahedral geometries. The strength and position of the latter hydrogen bonds play an important role in the Mn_3CaO_4 electronic structure and in our proposed mechanism. Ideal tetrahedral geometry imposes sp^3 hybridization of the valence oxygen orbitals, essentially eliminating π bonding to Mn and yielding longer and weaker Mn–O bonds. Such bonding is less directional and thus more flexible than, for example, $Mn_3(\mu_3\text{-O})$ in planar geometry, which has stronger $sp^2 + p_z$ (multiple) bonding and is more inflexible (6). As a result of this bonding dichotomy, two geometrical limits exist for Mn_3O_x core types among inorganic complexes: an incomplete cubane-$Mn_3(\mu_3\text{-O})_4$ and planar-$Mn_3(\mu_3\text{-O})(OH)_3$. Prevention of planarization is essential for high water oxidation activity in Mn_4O_4 model complexes. In the WOC, Ca^{2+} helps prevent planarization of Mn_3O_4 by binding to three corner oxos, completing and stabilizing the heterocubane topology (see Photoassembly of PSII Water-Oxidizing

Complex). However, owing to its filled valence electronic configuration, Ca^{2+} has no directional bonding preference at all (ionic bonding). Hence, the oxos coordinated to Ca^{2+} are much less positionally constrained, contrary to the case of a Mn_4O_4 cubane (6). This added flexibility of the Mn_3CaO_4 heterocubane is believed to be a major reason for the WOC's high catalytic activity, as it facilitates the proposed rate-limiting O-O bond formation step between oxos (48). It may also help rationalize the unusual WOC structure observable in the Umena et al. (17) XRD structure, which some characterize as distorted or damaged by X-rays.

Oxygen atom O4 covalently bridges the heterocubane subcluster to the exocuboidal Mn4. This Mn has historically been denoted the dangler (49) or gateway (50) Mn, in reference to its magnetic or redox properties, respectively. Mn4 plays a crucial role in the photoassembly of the WOC (see Photoassembly of PSII Water-Oxidizing Complex, below). O4 is bound to two Mn atoms (Mn3 and Mn4) and strongly hydrogen bonded to a water molecule (W539, 2.55 Å) positioned in the same plane at a trigonal planar site (μ_3-oxo). This geometry and bond length show that O4 is sp^2 hybridized and hence participates in strong covalent π bonding between Mn3 and Mn4. O4 is surrounded by a constellation of five hydrogen bonds within 3.3 Å (three Asp and CP43-R357), suggestive of a proton transfer network. This bonding arrangement is conducive to tautomerization between O4 and the water molecule W2 located *trans* to O4 (see Donor-Side Kinetics, below), as found in *trans* oxo/hydroxo Mn complexes (51, 52). This tautomerization equilibrates these two forms, O-Mn4-W2 $\Leftrightarrow$ HO-Mn4-OH(W2) and implies resonance stabilization of W2 resulting from stronger (π) bonding. This interpretation is supported by its short Mn4-O bond length (2.2 Å) and exceptionally low positional disorder (threefold-smaller volume than all other oxos!) (17).

As previously stated, the bonding environment around O5 is most unusual. O5 has 4 + 0 ligands (no ordered H-bonds) and is denoted μ_4-oxo. Its geometry is an incomplete octahedron missing two coordination sites *trans* to vectors Mn3-O5 and Ca-O5. This bonding environment indicates that the O5 orbitals are unhybridized and comprise valence s + 3p atomic orbitals directed at the metals and at two open (uncompensated) sites on the octahedron. This geometry is compatible with the possibility that O5 may be a hydroxide ion (protons are not detected in XRD) but is not likely a water molecule. Additionally, the absence of structurally ordered hydrogen-bonding partners to O5 disfavors hydroxide or water at O5. The space *trans* to Mn3-O5 lacks positioned atoms until a methyl group 3.68 Å away (D1-V185) and is presumably filled with disordered water molecules. Similarly, the space *trans* to Ca-O5 lacks positioned atoms until a Cl^- (or HCl) 6.89 Å away. These features all point to an electron-deficient (nearly neutral) O5 atom or hydroxide with atomic s + p orbitals occupied with bonding and antibonding electrons from neighboring metals, resulting in very long bond lengths and an unusual incomplete octahedral geometry. The flexibility of the heterocubane core would facilitate attaining this structure.

The Mn-Mn and Mn-Ca distances revealed by the Umena et al. (17) structure are clearly at odds with previously reported distances from extended X-ray absorption fine structure (EXAFS) measurements by Yano, Yachandra, and coworkers (53, 54). However, the geometry is strikingly similar to a model based on X-ray absorption spectroscopy (XAS) and XRD data by Dau and coworkers (55) and to a separate model based on density functional theory (DFT) calculations by Siegbahn (56, 57). The inherent flexibility of the heterocubane core geometry and intermanganese redox tautomerism have been proposed as a possible reconciliation (58, 59).

Umena and coworkers (17) took great care to minimize the X-ray dose per crystal unit volume. However, some photoreduction of $Mn^{3+/4+}$ to Mn^{2+} is expected from exposure to 13.3 keV (0.9 Å) radiation. Yano and coworkers (60) showed that a PSII crystal with 61% H_2O content contains, on average, approximately

20% Mn^{2+} during exposure to 0.28×10^{10} photons μm^{-2} (at 100 K, 13.3 keV, the maximal dosage reported by Umena et al.). These values are based on XANES (X-ray absorption near edge structure) calibration standards. The final Mn^{2+} content in the Umena et al. structure is likely less given that their crystals were dehydrated to 57% H_2O (17). Dau and coworkers (61) found similar results suggesting photoreduction in XRD methods. Previous XRD structures were exposed to much higher X-ray doses. For example, the 3.5-Å resolution structure by Ferreira et al. (15, 60) was exposed to 1.75×10^{10} to 3.5×10^{10} photons μm^{-2} (at 100 K, 13.3 keV). At this dosage, approximately 50–70% of $Mn^{3+/4+}$ was reduced to Mn^{2+}, on average (60). Paradoxically, the overall WOC geometry ($CaMn_3O_4$ heterocubane plus an exocuboidal Mn4) is quite consistent between the 3.5-Å Ferreira et al. structure and the 1.9-Å Umena et al. structure despite the 6–12-fold difference in X-ray exposure and 2.5–3.5-fold difference in predicted Mn^{2+} content. To us, this suggests that although photoreduction may be occurring, photodamage is not significantly distorting WOC geometry.

By comparing the Mn-Mn distances in the 1.9-Å XRD structure with EXAFS spectra (53, 62, 63), several groups have calculated that the crystal structure reflects a reduced S state lower than S_1 (64–67). This conclusion is based on the assumption that the average oxidation state of Mn is +3.5 in S_1. However, if a lower oxidation state assignment is used (Mn^{3+} average in S_1), DFT calculations suggest that the Umena et al. WOC geometry can be readily explained without photoreduction arguments (see sidebar, Mn Oxidation States in PSII: An Ongoing Debate) (58). The foregoing structural analysis is developed in A Proposed Mechanism for Water Oxidation, below.

PHOTOASSEMBLY OF THE PSII WATER-OXIDIZING COMPLEX

The Mn_4CaO_5 WOC core is not chemically stable as a free cofactor and must be assembled within the PSII-apo-WOC complex using energy derived from PSII charge separation. During biogenesis, the native inorganic cofactors Mn^{2+}, Ca^{2+}, and Cl^- bind to the apo-WOC domain of the newly translated and modified PSII protein scaffold and, through a sequence of light and dark steps, assemble the O_2-evolving complex (68, 69). Bicarbonate serves as a native cofactor in plant PSII and accelerates the kinetics of this slow process (70), exerting an influence on water oxidation kinetics through the arginine residue CP43-R357 in the holoenzyme (71). This maturation process, historically known as photoactivation (12, 68), occurs naturally during de novo biogenesis of PSII and repair of damaged PSII centers. Photoinactivation of PSII is a natural process that occurs across all phylogenetic species of oxygenic phototrophs during O_2 evolution at high light flux. It involves irreversible damage to the D1 subunit, which binds the WOC (40). Photoinactivation would limit photosynthetic productivity without the repair process, in which the PSII complex is recycled by removal of the damaged D1 and replacement with a new copy, followed by photoassembly of a new WOC (reviewed in Reference 12).

The pioneering work of Cheniae and coworkers (69, 72–74) showed that photoassembly is a multiquantum process, and the basic kinetic scheme derived from these original studies on spinach PSII membranes remains intact, although the molecular details have been significantly extended (**Figure 3**) (12, 75–78). Beginning from a dark-adapted PSII-apo-WOC precursor plus inorganic cofactors (IM_0), photoassembly starts by photooxidation of one Mn^{2+} to form intermediate IM_1, which then undergoes an essential dark-rearrangement step to form IM_1^* before further productive photooxidation can continue (**Figure 3**). Ca^{2+} affinity increases during this dark step, and Ca^{2+} addition specifically accelerates this step (79–81). Electron paramagnetic resonance (EPR) spectroscopy has revealed that this interaction involves binding to form a shared bridging (hydr)oxo ligand between Mn^{3+} and Ca^{2+} (82). The formation of IM_1 has a very low quantum yield (~0.25%).

S_i: Kok-cycle intermediate ($0 \leq i \leq 4$)

Electron paramagnetic resonance (EPR): spectroscopic technique used to study changes of the spin states of unpaired electrons

Mn OXIDATION STATES IN PSII: AN ONGOING DEBATE

Based upon the multiline EPR signals of the S_2 and S_0 Kok-cycle intermediates, all four Mn ions of the WOC are electronically coupled to produce a single set of cluster electronic states with spin multiplicity of S = 1/2 (160, 161). Additionally, EPR, ^{55}Mn-ENDOR (electron-nuclear double resonance), and XAS spectroscopic analyses agree that S_2 contains a combination of Mn^{3+} and Mn^{4+} (49, 162–165). Therefore, the catalytic cycle of water oxidation begins with S_0 as either $Mn^{2+}(Mn^{3+})_3$ [low oxidation state (LOS) assignment] or $(Mn^{3+})_3Mn^{4+}$ [or equivalently $Mn^{2+}Mn^{3+}(Mn^{4+})_2$] [high oxidation state (HOS) assignment].

The HOS paradigm is preferred by many in the field based on its interpretation of the PSII Mn K-edge (63, 166–170), Mn Kβ (59, 169, 171), and RIXS (K pre-edge) (54, 172) spectroscopic features when compared with model compounds. For a detailed analysis of these studies, see the recent review by Pace and coworkers (173). ^{55}Mn-ENDOR data suggest that Mn^{2+} is not present in S_0 and therefore support the HOS model (174, 175). This conclusion is based on the relatively narrow S_0 spectral envelope (attributable mainly to ^{55}Mn magnetic hyperfine terms) compared with octahedral Mn^{2+} complexes used as references (invariably large magnetic hyperfine). However, the ligand field symmetry around Mn4 is not octahedral according to the XRD structure of S_1 (**Figure 1**). Rather, it is five-coordinate (the Mn_4-O_5 distance, 2.5 Å, is too long for appreciable bonding character) and lacks inversion symmetry, an essential requirement to observe large scalar ^{55}Mn hyperfine interactions (176). Therefore, we propose that the Mn^{2+} model complexes used to calibrate this assignment may not accurately reflect the ligand field or the ^{55}Mn hyperfine interactions found at the Mn4. This suggestion needs more evidence going forward.

Two methods have been used to count the number of charge equivalents in the PSII-WOC. Yocum and coworkers (177) titrated intact PSII-WOC samples with excess chemical reductants and observed the loss of O_2 evolution activity and the release of Mn^{2+}. Their data suggest S_1 is present as $(Mn^{3+})_2(Mn^{4+})_2$ (HOS assignment). However, the reductants utilized (specifically hydroxylamine) interact with and reduce other species besides $Mn^{3/4+}$ (178, 179). In contrast, our group has determined the number of quanta of light (STFs) required to photoassemble apo-PSII-WOC starting from Mn^{2+} and Ca^{2+}. Two studies utilizing different flash intensities and durations have found that O_2 is first released after seven flashes (one-electron transfer steps) (79, 86). These results correspond to the LOS S_1 assignment of either $(Mn^{3+})_4$ or $Mn^{2+}(Mn^{3+})_2Mn^{4+}$. We emphasize that titration and photoassembly methods do not rely on model complexes for calibration. Hillier & Wydrzynski have also argued for the LOS assignment of S_1 [$(Mn^{3+})_4$] based on the comparison of water exchange kinetics in Mn^{3+}-containing model complexes and PSII (180). More experiments are needed to fully resolve this critical debate in PSII research.

Additionally, IM_1 decays if the light flux is very low, or is unproductively photooxidized if the dark process does not complete first. EPR spectroscopic data support all of the suggested structures for IM_0, IM_1, and IM_1^* in **Figure 3** (83). The next intermediate, IM_2, forms by photooxidation of a second Mn^{2+}. The structure in **Figure 3** is only postulated as no direct spectroscopic evidence currently exists to characterize IM_2. All light-induced intermediates after IM_1^* form with much higher quantum yield and have not yet been isolated for characterization.

Experiments by Burnap and coworkers (84) using cyanobacterial cells have used paired

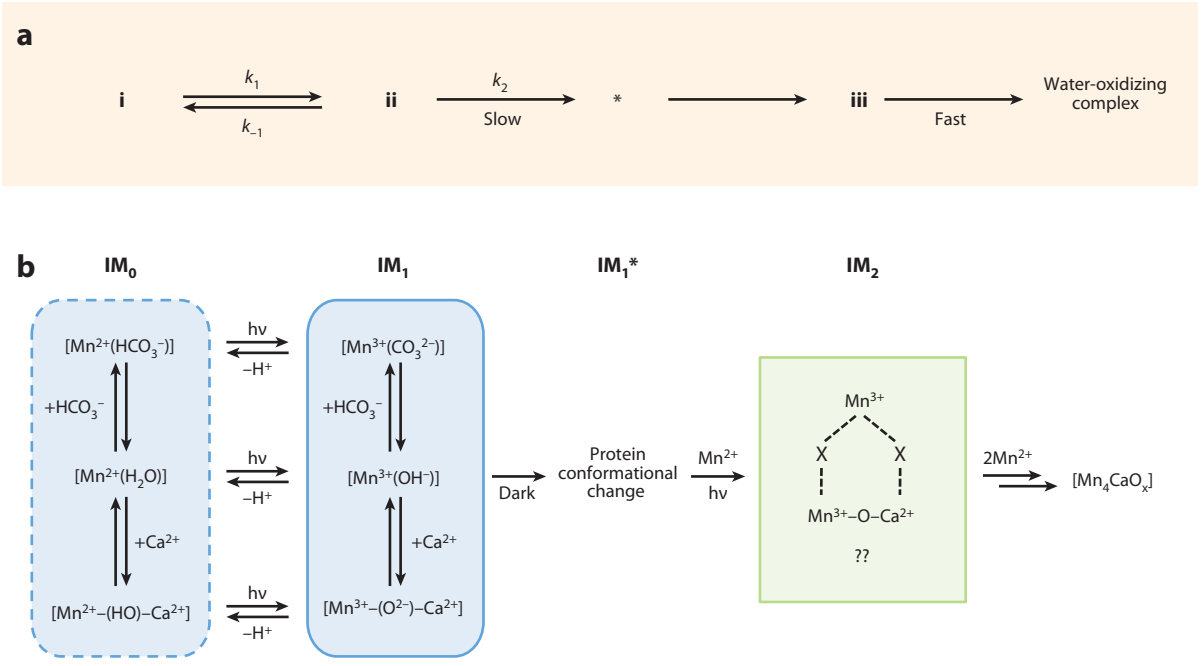

Figure 3

The sequence of kinetic intermediates (panel *a*) and proposed chemical formulation (panel *b*) of the intermediates formed during the major photoassembly pathway in spinach photosystem II membranes. Figure adapted from Reference 12.

flash experiments to reveal a third kinetic phase of photoassembly in a minority of centers, presumably representing an alternate pathway to the second intermediate, IM_2. The rate to this intermediate is 5–10 times faster than the rate-limiting dark-rearrangement step that is normally observed in plant PSII. Assuming that the dark-rearrangement step is a protein conformational change, Burnap and coworkers propose the possibility that a fraction of the centers may already exist in the rearranged state during or shortly after the first light-induced step. These centers are thus able to process the second quantum without the prior delay required by the conformational change. Burnap's observation fits well with photoassembly measurements using spinach PSII membranes, in which Ca^{2+} was replaced by Cd^{2+}, an inhibitor of O_2 evolution (85). This change produces a tenfold acceleration of the dark step in Cd^{2+}-reconstituted centers, which bind competitively and more strongly to the native Ca^{2+} site. Apparently, the low Ca^{2+} affinity thus controls the rate of the slow dark conformational step, and some other cations that bind more tightly (e.g., Cd^{2+}) accelerate conversion to the ready state, IM_1*. Subsequently, photoassembly proceeds, and Cd^{2+} can be exchanged with Ca^{2+} to yield catalytically competent WOC (85).

The three kinetically resolved steps of photoassembly are associated with cofactor uptake by an ordered sequence of steps $1Mn^{2+}$(1 photon) + Ca^{2+}(dark) + $3Mn^{2+}$(*n* photons), as illustrated in **Figure 4**. The dark step is gated by Ca^{2+} and appears to involve a protein conformation change (D1 carboxyl terminus?) that controls the kinetics (86). This step templates the formation of the binding site for the remaining three Mn ions. Without Ca^{2+}, many more than three Mn^{2+} ions bind and photooxidize to form an unproductive intermediate (87).

The Mn^{2+} and Ca^{2+} stoichiometries, their cooperative binding, and their kinetic sequence of uptake as determined by photoassembly

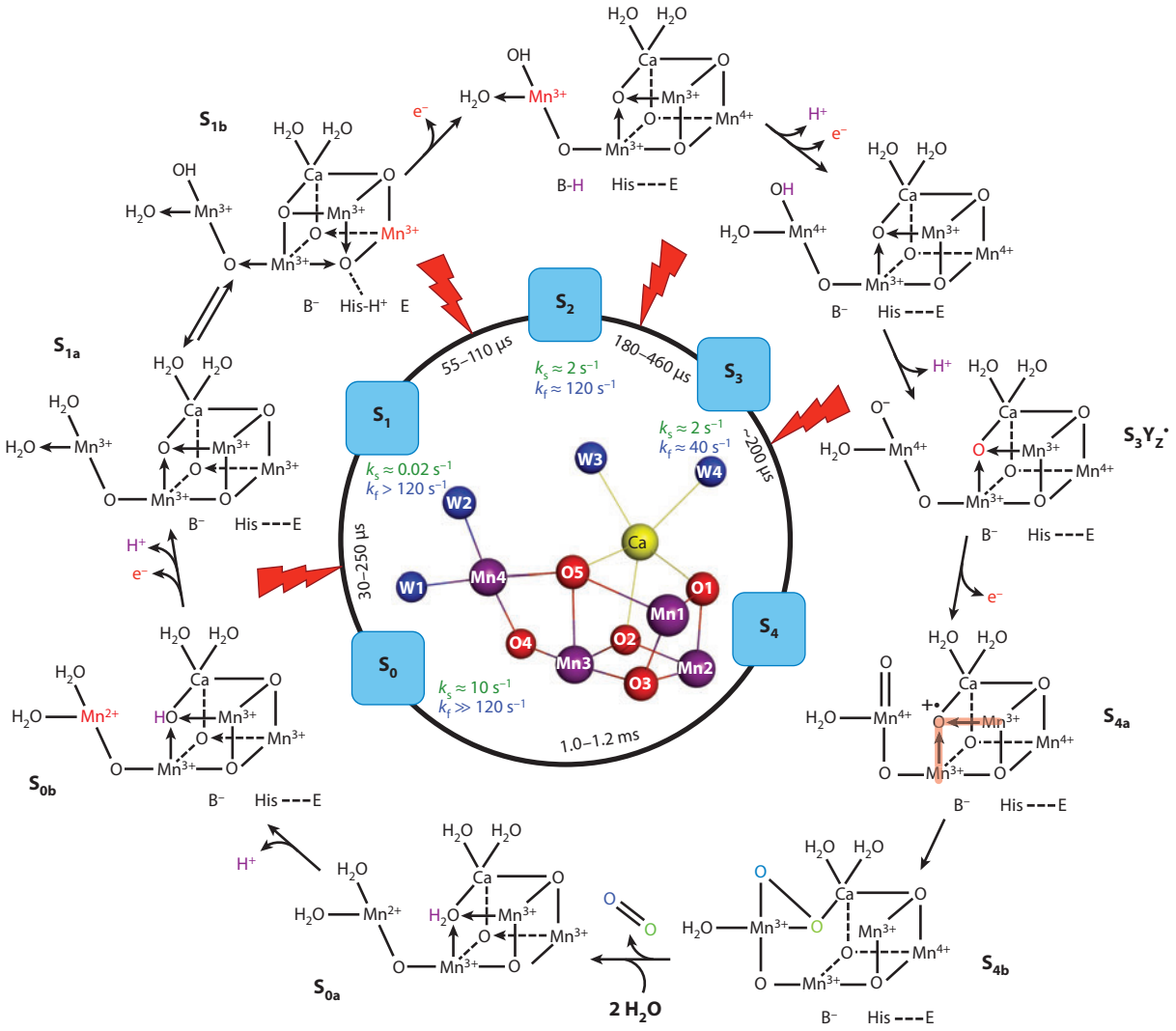

Figure 4

Proposed mechanism of water oxidation by the photosystem II (PSII) water-oxidizing complex (WOC). Arrows within chemical structures represent the alignment of the Jahn-Teller axis on each Mn^{3+}, corresponding to the antibonding $e_g^1(d_{z2})$ orbital. Rate constants for S-state transitions (*black text*) are detailed in **Table 1**. Fast and slow substrate water exchange rates (k_f and k_s, respectively) were measured at 10°C in spinach PSII membranes (186, 187). The inset structure of the PSII-WOC is analogous to intermediate S_{1b} in our mechanism and was generated in the PyMOL program using coordinates from Protein Data Bank entry 3ARC (17).

actually forecast the structural organization of these cofactors in the WOC, as seen in recent XRD studies (reviewed in References 12, 75). The initial Mn^{2+} site, corresponding to Mn4, was further identified as the dangler Mn by EPR spectroscopy of the holoenzyme (49). EPR spectroscopy of photoassembled cyanobacterial PSII-apo-WOC core complexes has given further evidence describing the ligand field of $(Mn4)^{3+}$ in IM_1 (88). A μ-oxo (formally μ-oxido or di-μ-hydroxido) bridge forms between Mn^{3+} and Ca^{2+} during photoassembly, as identified by EPR spectroscopy (82). This appears to be the O5 bridge from Mn4 to

Ca^{2+} (**Figure 1**). During photoassembly, Ca^{2+} locked in a fixed ligand field at $(Mn4)^{3+}$ independent of the solution pH; in the absence of Ca^{2+}, this $(Mn4)^{3+}$ ligand field varied systematically with pH. Thus, a critical role of Ca^{2+} is to work together with $(Mn4)^{3+}$ to form an ionized oxide bridge (O5) that is chemically and kinetically stable over a wide pH range and provides the template for the cooperative binding and high-quantum-yield photooxidation of the remaining three Mn^{2+} (82). These remaining steps assemble the Mn_3O_4-incomplete cubane to the precursor [(Mn4)(O5)Ca], forming the Mn_4CaO_5 catalytic core (see Structure, above).

Chloride is essential for O_2 activity of PSII (89) but not for photoassembly (12). Although no protein chaperones are required for photoassembly (the process can proceed in vitro with purified apo-PSII-WOC), (bi)carbonate is an important cofactor that accelerates the rate and increases the yield of photoassembly. During photoassembly of spinach PSII, it acts through two binding sites: One is a general base site, and the other is specific to (bi)carbonate (70, 80). Electron spin-echo envelope modulation (ESEEM) studies of ^{13}C-bicarbonate binding established that the latter interaction involved direct coordination to $(Mn4)^{2+}$ and contributed to the ligand field around $(Mn4)^{3+}$, possibly by delivery of (hydr)oxide for formation of a μ-oxo bridge to Ca^{2+} (90). Although (bi)carbonate appears not to be essential for O_2 evolution activity in some PSIIs (91), it significantly influences the kinetics of O_2 evolution in a cyanobacterial strain mediated by CP-R357 (71) and is absolutely essential for the operation of hypercarbonate strains (21), in which it appears to be important for proton evolution (92).

A PROPOSED MECHANISM FOR WATER OXIDATION

Next we propose an atomic mechanism for water oxidation that uses the low oxidation state assignment and builds on a prior mechanism that adopted this assignment (48). We apply the results highlighted in other sections of this review, the atomic positions taken from the 1.9-Å structure (17), and recent DFT calculations. Two remarkable features of the XRD structure that we develop in our proposed mechanism are the unusual ligand field at O5 and the very highly ordered W2 (threefold-lower positional disorder). In our mechanism, we suggest that these two oxygens are derived from substrate waters by applying the principles of chemical bonding and reactivity from inorganic chemistry (93). Notably, we explicitly include the consequences of the Jahn-Teller (JT) effect. This vibronic term causes tetragonal elongation around Mn^{3+} owing to distortion around the asymmetric electronic configuration (d_{x2-y2} hole and antibonding electron in d_{z2}) and results in a large energy stabilization of 0.5–1 eV for Mn^{3+} in oxide ligand fields (93). This effect cannot be overlooked in chemically accurate mechanisms. We also include the mechanistic and energetic consequences of the proton ionization of water molecules bound to $Mn^{2+/3+/4+}$ cations (pK_a differences). Notably, a factor of seven to eight difference in pK_a exists for water molecules bound to axial versus equatorial positions of JT-distorted Mn^{3+} (94). These terms are critical to account for the large differences in substrate water exchange rates with the S state, as determined by ^{18}O-isotope mass spectrometry (95). To our knowledge, the S-state dependence of these rates has not been successfully incorporated within any self-consistent mechanism.

Jahn-Teller (JT) effect: tetragonal elongation of six-coordinate Mn^{3+} ($3d^4$) resulting from asymmetric electronic configuration (hole in d_{x2-y2} and antibonding electron in d_{z2})

Flash #1: $S_1 \rightarrow S_2$

We begin with the dark-stable S_1 intermediate in the low oxidation state $(Mn^{3+})_4$ (**Figure 4**). In our model, S_1 can exist as two proton tautomers as recently hypothesized by Pace and coworkers (96). The first S_{1a} species (derived from S_0) features W2 as an aqua ligand to Mn4. Based on energetics (93) and by analogy to those observed from a $(Mn^{3+})_4O_4$ model cubane (97), the JT axes of Mn1 and Mn3 are predicted to point toward O5 and that of Mn2 is predicted to point toward O2 in S_{1a}. The other (preferred) tautomer S_{1b} is predicted to form upon net movement of a proton from W2 [bound at the more acidic non-JT axis on

Y_Z: tyrosine residue D1-Y161

$(Mn^{3+})_4$] to D1-H337. This is likely mediated by the water network connected to W2 and by an internal proton donor, BH. S_{1b} is driven to tautomerization by coordination of the protonated imidazoyl cation on H337 to O3 via a strong hydrogen bond [2.6 Å in the Umena et al. structure (17)]. This tautomerization drives the reorientation of the JT axes of Mn1 and Mn3 toward O3. The S_{1b} vibronically stabilized tautomer can explain the decrease in substrate water exchange rates measured by Hillier & Wydrzynski (**Figure 4**; reviewed in Reference 95). As shown in **Figure 4**, the rearrangement of two JT axes in tautomer S_{1b} produces a more tightly bound O5 owing to the loss of two antibonding interactions from Mn1 and Mn3. This stronger bonding is consistent with the observed 500-fold slowing of the substrate exchange rate in S_1 relative to the (OH)5 exchange rate in S_0 (**Figure 4**), assuming that O5 is the slow-exchanging substrate water site.

Species S_{1b} continues in our proposed catalytic cycle. Following photochemically driven charge separation, $Y_Z^\bullet$ oxidizes Mn2 ($Mn^{3+} \rightarrow Mn^{4+}$), triggering the following steps: (*a*) internal movement of a proton from the histidyl cation H337-H^+ to a base B^- caused by the loss of an electron and stronger covalent bonding within the Mn2(O1)(O3)Mn1 rhombus [the $(Mn1)^{3+}$ d_{x2-y2} hole is directed at O1 and O3, and d_{z2}^1 is pointed at O5], and (*b*) reorientation of the JT axis on Mn3 along O5 to accommodate this stronger covalent bonding. As a result of this realignment of two JT axes with their antibonding interactions directed at O5, the water exchange rate of O5 is predicted to increase substantially from its S_1 value, consistent with the experimental data showing a 100-fold increase at the slow substrate site in S_2 (**Figure 4**). The faster exchanging site (W2) is not directly affected and slows by a much smaller value (**Figure 4**).

Flash #2: $S_2 \rightarrow S_3$

After the second flash, a rapid deprotonation event is followed by a metal-centered oxidation (98). This redox-leveling process partially mitigates the energy barrier of the second oxidation by decreasing the formal charge of the WOC. We propose that the internal base BH associated with H337 (**Figure 4**) is deprotonated to the bulk in this step. Neutral H337 may be stabilized by hydrogen bonding to the backbone carbonyl of E333 [noted as E in **Figure 4** and located 3.37 Å from H337 in the Umena et al. structure (17)]. The hole injected into the Mn_4Ca cluster by $Y_Z^\bullet$ is postulated as localized to Mn4 ($Mn^{3+} \rightarrow Mn^{4+}$). Thus, the fast-exchanging water (W2) should bind more tightly than in the previous intermediate, and the bonding environment of the slow-exchanging site (O5) is not significantly affected in the $S_2 \rightarrow S_3$ transition (**Figure 4**).

Flash #3: $S_3 \rightarrow S_4 \rightarrow S_0 + O_2$

O_2 is released following the third flash through a complex series of intermediates. First, we propose that the formation of $Y_Z^\bullet$ facilitates the deprotonation of W2 to the bulk via the adjacent water network (species $S_3Y_Z^\bullet$ in **Figure 4**). Next, the $Y_Z^\bullet$ hole is subsequently transferred to the cluster, generating an oxyl radical cation at O5 (S_{4a}) that is stabilized by delocalization of the hole between the antibonding d_{z2}^1 electrons on Mn1 and Mn3, as highlighted in **Figure 4**. Ultimately, this configuration evolves to form a bond between O5 and Mn4, as shown in **Figure 4**.

The O5 oxyl radical is in close proximity to the terminal oxo of Mn4 (W2). Terminal O-Mn^{4+} bonds *trans* to oxido (O4) are uniquely weak (and long) owing to a half-filled d_π^3 shell with three antibonding electrons (99). This configuration favors formation of an intramolecular O-O bond, shown as the peroxo intermediate S_{4b} in **Figure 4**. The peroxo intermediate that forms at Mn4 in our mechanism is formally similar to the peroxo intermediate that forms during O_2 release from permanganate (MnO_4^-) following photoexcitation in the gas phase (100, 101). Based on DFT calculations and assuming the high oxidation state assignment, Siegbahn (67, 102) found that an oxo-oxyl radical coupling mechanism for O-O

bond formation in S_4 has significantly lower energy than the nucleophilic attack mechanisms preferred by Brudvig and coworkers (103). Importantly, spin states are consistent with bond formation in the Siegbahn oxo-oxyl radical coupling mechanism. The unpaired electron on O5 is predicted to have spin β, which would populate a bonding orbital with a spin α electron from the oxo of Mn4 (102). In a seminal recent paper by Lubitz and coworkers (104), a bridging oxo (O5) was shown to be exchangeable at rates compatible with those previously reported for substrate water exchange (95), which leads directly to possible oxo-oxyl radical coupling mechanisms involving O5, as shown here.

Conversion to O_2 by internal charge transfer is downhill in energy (105, 106). O_2 is released upon uptake of the next two substrate water molecules at sites W2 and O5 (S_{0a} in **Figure 4**). In the resulting S_{0b} state, the water molecule at position O5 spontaneously deprotonates via the adjacent water network to the bulk, forming a μ_3-hydroxide ligand that assumes sp^3 hybridization with weak bonds to Mn1 and Mn3 and ionic association with Ca^{2+}. There is no appreciable bond strength between Mn4 and O5 in S_0, in agreement with the long 2.5-Å distance seen in the XRD structure of S_1 (17). This conformation of S_0 results in the fastest exchange rate of the slow substrate water site (O5, 10 s^{-1}; **Figure 4**). The fast-exchanging water (W2) is bound to $(Mn4)^{2+}$ and also exhibits its most rapid rate in S_0 (>120 s^{-1}; **Figure 4**).

Flash #4: $S_0 \rightarrow S_1$

Following the fourth flash, a metal-based oxidation step precedes deprotonation (98). We propose that the five-coordinate Mn4 is oxidized from Mn^{2+} to Mn^{3+} in this step. The final deprotonation event is centered at O5, and during it the hydroxo is converted to a corner μ_3-oxo weakly bridging Mn1, Mn3, and Mn4 and ionically associated with Ca^{2+}. As previously discussed, the absence of ordered hydrogen-bonding partners of O5 in the Umena et al. (17) structure suggests that O5 is more likely a bridging oxo rather than a hydroxo in S_1.

Additional Considerations

The foregoing mechanism emphasizes the most recent structural, electronic, and chemical attributes of the WOC, specifically the oxygen atomic coordinates, the lower oxidation state, and water exchange rates. We stress that our proposed mechanism for WOC turnover, although based on established principles of chemical bonding within transition metal–oxo complexes, may need further refinements from consideration of other experiments or computations.

P_{680}: reaction center Chl *a* dimer

DONOR-SIDE KINETICS

The redox-active tyrosines Y_Z (D1-Tyr161) and Y_D (D2-Tyr160) are located symmetrically in the D1 and D2 subunits of the homodimeric reaction center core, nearly equidistant to P_{680}; Y_Z is between P_{680} and the $CaMn_4$ site (**Figure 5**). They have been extensively researched (107). Their environments are highly ordered with different residues and water accessibility that confer different electrochemical potentials, as understood from synthetic models (108). For example, only $Y_Z^{\bullet}$ has sufficient thermodynamic driving force to advance all S-state transitions of the Kok cycle, whereas Y_D actually acts as an inefficient reductant to the S_2 and S_3 states (109–111). These differences account for their substantially different kinetics of electron donation to the Mn_4CaO_5 complex. The kinetics of the reduction of P_{680}^{+} by Y_Z are triphasic and have time constants of 20–50 ns (fast nanosecond kinetics), 300–600 ns (slow nanosecond kinetics), and 30–35 μs (microsecond kinetics) (112–115). The fast nanosecond kinetic reaction is facilitated by a hydrogen-bonding interaction between Y_Z (hydroxo) and D1-His190. The two slower kinetic reactions are related to changes in the protein environment that favor Y_Z oxidation. The 300–500-ns kinetic reaction is controlled by changes in the local dielectric protein environment, whereas the 30–35-μs kinetic reaction reflects proton rearrangement processes. The energetics of these relaxation processes contribute

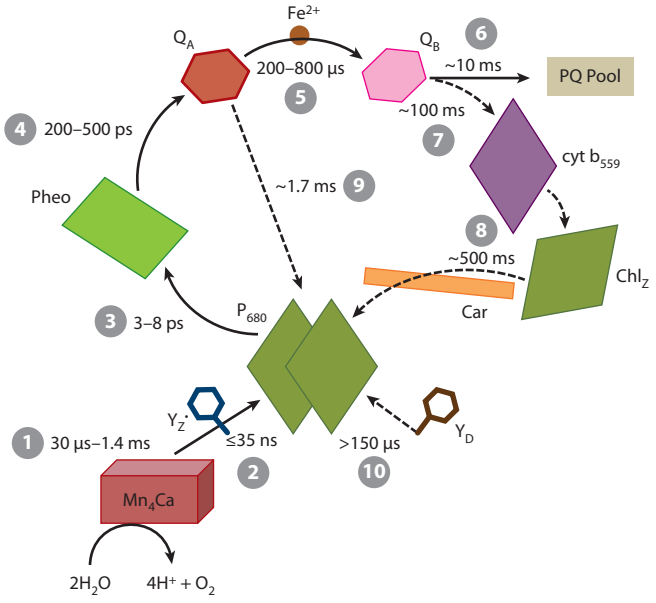

Figure 5

Kinetics of electron/hole carriers in photosystem II (PSII). Dotted lines represent secondary electron transfer pathways as described in Light to Chemical Conversion Efficiency in PSII. ❶ $Y_Z^{\bullet}$ oxidation kinetics are S-state dependent, as detailed in **Table 1**. ❷ The reduction of P_{680}^+ by $Y_Z^{\bullet}$ is multiphasic (112–115). ❸ The reduction of Pheo (188–190) is approximately 100-fold faster than the ❹ subsequent reduction of Q_A (188, 190–192). ❺ Q_B accepts two electrons from Q_A (τ = 200–400 µs for $Q_A^- Q_B \rightarrow Q_A Q_B^-$ and 500–800 µs for $Q_A^- Q_B^- \rightarrow Q_A Q_B^{2-}$) (134–137). ❻ Q_B preferentially exchanges with the PQ pool (193) or ❼ can reduce cyt b_{559} (194). ❽ P_{680}^+ can be reduced via the network of Car, Chl_Z, and cyt b_{559} (195). ❾Alternatively, P_{680}^+ can be reduced by direct charge recombination (quantum tunneling) with Q_A (150). Indirect (nonradiative) recombinations of $[P_{680}^+ Pheo^-]^1$ and $[P_{680}^+ Pheo^-]^3$ occur with half-times of >1 ns and ~200 ps, respectively (151, 196). ❿ The reduction of P_{680}^+ by Y_D has a half-time of >150 µs at pH 6.5 (142). The oxidation of S_0 by $Y_D^{\bullet}$ is much slower and occurs on the order of 5–40 min (111). Abbreviations: Car, carotenoid; PQ, plastoquinone.

approximately 0.1 eV of stabilization energy for this reaction, with contributions of 10, 25, and 60 meV for each of the three phases, respectively (116). Renger & Renger (13) noted that the contribution of the slower phases increases upon replacement of Ca^{2+} by Sr^{2+} in the Mn_4Ca site, revealing that the relaxation-dependent phases of Y_Z oxidation involve degrees of freedom extending to the inorganic core.

The kinetics of individual S-state transitions and the O_2 release rate are considerably faster than the catalytic turnover rate, which is typically limited on the acceptor side by reoxidation of $(PQH_2)_B$. The kinetics of $Y_Z^{\bullet}$ reduction and Mn oxidation in the WOC center have been analyzed by time-resolved EPR spectroscopy (117, 118) and optical changes in UV absorption (119). These data show that $Y_Z^{\bullet}$ is the direct oxidant of Mn during S-state transitions. The time courses for the one-step advancements of S_0, S_1, and S_2 satisfy single exponential kinetics, in contrast to the multiphasic Y_Z oxidation by P_{680}^+ (see above). The half-lives of these reactions are given in **Table 1** and reflect the kinetics for resting populations in dark-adapted PSII. The rates of $S_0 \rightarrow S_1$, $S_1 \rightarrow S_2$, and $S_2 \rightarrow S_3$ as measured by EPR and XAS progressively slow in the ranges of 30–70 µs, 70–110 µs, and 180–350 µs, respectively (63, 117, 118). Interestingly, the $S_0 \rightarrow S_1$ transition is supposedly slower than $S_1 \rightarrow S_2$ when UV absorption or FT infrared spectroscopy (FTIR) absorption is used to monitor the reaction kinetics (119, 120). The S_3 oxidation by $Y_Z^{\bullet}$ is slower by a factor of three to eight compared with the next slowest S-state transition and is the most sensitive to environmental factors. This step has been examined by time-resolved Mn XAS and FTIR and found to resolve into two phases with a lag phase of approximately 200 µs. The latter step correlated with the detection of proton release by an entropically favorable process (63, 120).

Kinetic data have been obtained for the detection of the released O_2 product in solution using electrochemical (18, 121, 122), EPR (123), and photoacoustic (124) methods (**Table 1**). Because diffusion lengths to the detector and internal sinks for O_2 solubility need to be considered in whole cells, data from isolated PSII complexes are considered more reliable for determination of the intrinsic half-life for O_2 release. The ranges of values found are 1.2–2.2 ms for polarography, 1–2 ms for EPR, and approximately 2 ms for photoacoustic methods. These rates are fully consistent with predicted kinetics of the $S_0 \rightarrow S_3$ transition. The release of O_2 is not reversible even at elevated O_2 pressure (125) and exhibits a driving force of at least 220 mV (126).

Table 1 S-state transition half-lives as measured by EPR (Y_Z reduction), UV absorption, X-ray absorption, and FTIR as well as O_2 release as measured by polarography, EPR, and photoacoustics

S-state transition half-life	EPR[a]	UV[b]	XAS[c]	FTIR[d]	Polarography	Photoacoustics
$S_0 \rightarrow S_1$	30–70 μs	250 μs	≤30 μs	130 μs		
$S_1 \rightarrow S_2$	100–110 μs	55 μs	70 μs	65 μs		
$S_2 \rightarrow S_3$	180–350 μs	290 μs	190 μs	460 μs		
$S_3 \rightarrow S_0$	1.0–1.4 ms	1.2 ms	1.1 ms	1.4 ms		
O_2 release	1–2 ms[e]				1.2–2.2 ms[f,g]	~2 ms[h]

Data refer to dark-adapted samples using single-turnover flashes. Abbreviations: EPR, electron paramagnetic resonance; FTIR, Fourier transform infrared spectroscopy; XAS, X-ray absorption spectroscopy.
[a]$Y_Z^{\bullet}$ reduction (117, 118).
[b]Mn^{ox} formation (119).
[c]Mn^{ox} formation (63).
[d]H^+ and protein dynamics (120).
[e]O_2 detection via EPR-active spin probe (123).
[f]Reference 121.
[g]Reference 122.
[h]Pulsed photoacoustic time shift resulting from O_2 release (124).

ACCEPTOR-SIDE KINETICS

Following the formation of the primary charge-separated state, [$P_{680}^+Pheo^-$], $Pheo^-$ reduces the primary acceptor, Q_A, a tightly bound plastoquinone (**Figure 5**). The thermodynamic driving force of this step is defined by the relative midpoint potentials of $Pheo/Pheo^-$ and Q_A/Q_A^- and is controlled by the local protein environment. The Pheo hydrogen-bonding partner D1-130 is a Glu in plants and algae but may be either a Glu or Gln in cyanobacteria, depending on the expressed D1 isoform regulated by light intensity (40). Substitution of Gln for Glu at D1-130 changes the $E_m(Pheo/Pheo^-)$ by −33 mV in *Synechocystis* (127) and −17 mV in *Thermosynechococcus* (44, 128). The E_m of Q_A/Q_A^- also varies based on species (129), D1 isoform (130, 131), and herbicide occupancy of the Q_B pocket (132).

Although Q_A accepts only one electron at a time and no protons, the secondary PQ acceptor, Q_B, is reduced and protonated twice to form PQH_2. Electron transfer from Q_A^- to Q_B is facilitated by a nonheme iron (Fe^{2+}) equidistant between the two PQ molecules. The nonheme Fe^{2+} is ligated by a bidentate bicarbonate ligand [essential for efficient electron transfer (91)] and four His residues: D1-H215, D1-H272, D2-H214, and D2-H268 (17). Through computational studies, the E_m of Q_B/Q_B^- is predicted to be dependent on the protonation state of D1-H252 (133). D1-S264 forms a hydrogen bond to Q_B that facilitates forward electron transfer from Q_A^- only when D1-H252 is protonated (133). Q_B is reduced with kinetic time constants of 200–400 μs for the first transfer ($Q_A^- \rightarrow Q_B$) and 500–800 μs for the second transfer ($Q_A^- \rightarrow Q_B^-$) (134–137). The resulting $(PQH_2)_B$ diffuses from the binding pocket and is replaced by an oxidized Q_B from the membrane-soluble PQ pool.

SECONDARY ELECTRON TRANSPORT WITHIN PSII

The most efficient electron transfer pathway in PSII is the linear flow of electrons from water to $(PQH_2)_B$ via the WOC, Y_Z, P_{680}, Pheo, Q_A, and Q_B. Although Y_Z is the preferred reductant of P_{680}^+, it is in competition with Y_D, Car (via cyt b_{559} and Chl_Z), and backward reactions from the acceptor side (e.g., Q_A^-). Additionally, although the combined impact of these secondary pathways (**Figure 5**) may be minimal under continuous moderate light flux, they

Q_A: primary PQ acceptor

Q_B: secondary PQ acceptor

Plastoquinone (PQ) pool: the membrane-soluble sum of oxidized PQ and reduced PQH_2

are essential for PSII survival under excess light fluxes and photoassembly (138).

Tyrosine D

Although the cation radical form of $Y_D^{\bullet}$ has a high reduction potential [E_m = 700–800 mV (111)], it remains oxidized in the dark for long periods and does not play a major role in PSII turnover under continuous illumination (107). However, Y_D is completely conserved in PSIIs from the genomes of all oxygenic phototrophs, indicating that it is absolutely essential. Owing to its hydrophobic protein environment, the $Y_D^{\bullet}$ radical is remarkably dark stable and can be observed via EPR for hours after exposure to light (139). However, Y_D can reduce both the S_2 and S_3 Kok-cycle intermediates (generated after one or two STFs, respectively) (109–111) but cannot reduce S_0 or S_1. Conversely, $Y_D^{\bullet}$ can oxidize S_0, although its kinetics are very slow (110, 111). These features help explain why after several minutes of dark adaptation, WOC centers are composed of approximately 25% S_0 and 75% S_1, but after many hours of dark adaptation, the population of S_1 approaches 100%. When P_{680}^+ formation is faster than WOC cycling or if the Mn_4Ca is disassembled, Y_D can directly reduce P_{680}^+ (140–142). This ability of Y_D to store an oxidizing equivalent supports photoassembly. The Y_D artificial mutant D2-Tyr160Phe was significantly impaired in the rate and yield of photoassembly of the WOC inorganic core (143).

Cyclic Electron Transport Around PSII: Cyt b_{559}, Chl_Z, and Car

The PsbE and PsbF subunits comprise the α- and β-subunits of cyt b_{559} and are essential components of the PSII core. As recently reviewed by Shinopoulos & Brudvig (138), following the formation of P_{680}^+, cyt b_{559} may be oxidized, and the oxidizing equivalent is rapidly equilibrated between cyt b_{559}, Chl_Z, and Car (144), and subsequently reduced by Q_B^-. This cyclic pathway around PSII functions when the Mn_4Ca cluster is not present, but it has also been observed experimentally in vivo in a photoprotective role under excess light conditions (145) when the PQ pool is highly reduced (146).

Charge Recombination

The initial [$P_{680}^+Pheo^-$] charge-separated state is short-lived and transfers to [$P_{680}^+Q_A^-$] within hundreds of picoseconds following photochemical excitation of P_{680} (147). Typically, Y_Z reduces P_{680}^+ and Q_A^- reduces Q_B. However, [$P_{680}^+Q_A^-$] may also recombine through various pathways with either photoprotective or destructive consequences [see excellent reviews by Vass & Cser (148) and Rutherford et al. (149)]. First, [$P_{680}^+Q_A^-$] may directly recombine via quantum tunneling. This nonradiative reaction is relatively slow (approximately 2 ms) and may serve a protective role in excess light conditions (150, 151). The free energy gap between Q_A/Q_A^- and P_{680}/P_{680}^+ is large (>1.2 eV). Thus, the relationship between the thermodynamics and kinetics of this recombination is hypothesized to follow inverted Marcus behavior owing to the predicted large reorganization energy (148). As previously discussed, the E_m of Q_A/Q_A^- varies considerably among species and cyanobacterial D1 isoforms (see Secondary Electron Transport Within PSII, above). Therefore, we and others have predicted that this tuning of the Q_A/Q_A^- E_m may be the result of evolutionary selection to maximize photoprotection and/or minimize inefficient back reactions under light-limited conditions (44, 45, 148, 149).

The [$P_{680}^+Q_A^-$] charge pair is in equilibrium with both the singlet and triplet states of [$P_{680}^+Pheo^-$] and can populate with different probabilities and consequences (132, 152, 153). Their formation is controlled by the free energy gap between Pheo/$Pheo^-$ and Q_A/Q_A^-. Similar to that of [$P_{680}^+Q_A^-$], the transient singlet state of ^{1}[$P_{680}^+Pheo^-$] decays harmlessly (and likely protectively) via a nonradiative direct pathway (148). In contrast, when triplet ^{3}[$P_{680}^+Pheo^-$] forms, it decays via triplet $^3P_{680}$, which, owing to its longer lifetime, may react with dissolved molecular oxygen, $^3O_2$, to form singlet

$^1O_2$. This product is a powerful oxidizing agent that causes extensive damage to PSII and surrounding sites (132, 152, 153).

LIGHT TO CHEMICAL CONVERSION EFFICIENCY IN PSII

PSII Reaction Center Efficiency

Here we focus on contributions to the solar energy conversion efficiency of PSII, η, which can be reduced to the product of three terms as in Equation 3 (4, 154),

$$\eta = \text{LHY} \times \text{FEY} \times \text{PQY}, \qquad 3.$$

where LHY is light-harvesting yield, FEY is fractional energy yield, and PQY is the quantum yield of product ($O_2 + PQH_2$) formation.

In PSII, individual quanta of visible light are absorbed directly or transferred from excited states of antenna pigments of comparable or higher energy and form the excited state of the photochemically active Chl, P_{680}^*. The yield of this reversible process depends on the product states (prior photochemical events) and defines the quantum yield for light harvesting by P_{680} (LHY). Estimates of maximum LHY for oxygenic phototrophs without product inhibition range from 34% to 50%, based on the full spectrum of incident solar radiation at the surface of Earth (3, 4). Subsequently, the excitation on P_{680}^* is trapped by photochemical conversion steps with a probability that depends on the product state (PQY). These occur as electron and proton transfer steps that form electron/hole pairs on specific neighboring cofactors. As depicted in **Figure 6** (from Reference 4) for PSII, the initial step involves forming a Chl *a* radical cation (P_{680}^+) and a reduced Pheo radical anion ($Pheo^-$). Also shown is the FEY relative to P_{680}^*, defined as the difference in their respective reduction potentials. This step is followed by a series of electron transfer steps to adjacent cofactors that further separate the electron/hole pair at the expense of further loss of internal energy in discrete amounts determined by the cofactor identity and environmental interactions. The FEY decreases overall by 0.49–0.58 V or 27–32% relative to P_{680}^* upon forward electron transfer on the acceptor side from $Pheo^-$ to Q_A^- to $(PQH_2)_B$. Likewise, on the donor side, sequential electron transfers to the high-potential hole of P_{680}^* are filled by Y_Z, which in turn oxidizes the WOC. There is an estimated overall energy loss of 0.32–0.44 V or 17–24% from P_{680}^* to the products in Equation 1*a* (4, 155). This results in a total FEY of 44–56% (ignoring the *pmf* created). This loss is a system design loss of PSII and is not an intrinsic overpotential specific to the WOC. These energy losses following the photochemical step (FEY) are the cost to ensure a high probability of charge transfer between each of the selected carriers and not others (PQY), while also suppressing wasteful charge recombination pathways (see Secondary Electron Transport Within PSII, above) (156). Another trade-off that the cofactor design must avoid is loss of excited state trapping at P_{680}^* and increased nonphotochemical quenching of P_{680}^* once it is formed. The magnitude of PQY is related to the turnover efficiency of WOC cycling (see below). Dark-adapted PSII with an oxidized PQ pool and donor-side proton buffers can achieve PQY of up to 95% ($1 - \alpha + \beta$) at low light fluxes (21), but the PQY is much lower even at ambient and certainly at full solar intensity as these reservoirs become filled, depending on the species. Returning to Equation 3, we estimate the maximal light to chemical quantum yield of PSII to be approximately 24% ($0.5 \times 0.5 \times 0.95$).

PSII–Water-Oxidizing Complex Cycling Efficiency

Most commonly, the efficiency of PSII is reported as a light-saturated rate of O_2 evolution that, when normalized to Chl content, approaches 6,000 μmol O_2 (mg Chl)$^{-1}$ h^{-1} in vitro (157). As shown in **Table 2**, the sustained turnover rates of the PSII-WOC vary considerably among cyanobacteria, algae, and higher plants and among PSII particle preparation methods. The historical units of μmol O_2 (mg Chl)$^{-1}$ h^{-1} can be converted

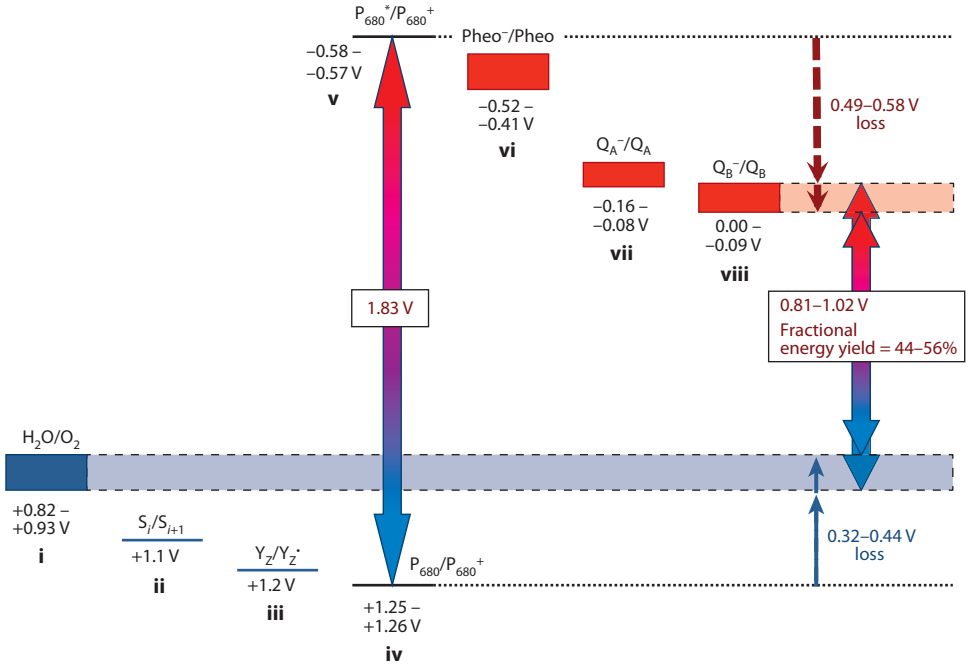

Figure 6

Relative energies of electron/hole carriers in photosystem II (PSII). Adapted from Reference 4. (i) $E_m(H_2O/O_2)$ values reflect the physiologically relevant pH range of 5–7. (ii) S-state E_m values were indirectly measured in spinach [+1.1 V (197)] or *Synechocystis* 6803 [+1.0 V (198)] with reference to an $E_m(Q_A^-/Q_A)$ value of −80 mV (199, 200). (iii) $E_m(Y_Z/Y_Z^\bullet)$ was indirectly measured in spinach (201) with reference to an $E_m(Q_A^-/Q_A)$ value of −80 mV (199, 200). (iv) $E_m(P_{680}/P_{680}^+)$ was indirectly measured in *Synechocystis* 6803 [+1.26 V (198)] or spinach [+1.25 V (201)] with reference to an $E_m(Q_A^-/Q_A)$ value of −80 mV (199, 200). (v) The $E_m(P_{680}^*/P_{680}^+)$ value is calculated as 1.83 eV (energy of a 680-nm photon) more negative than $E_m(P_{680}/P_{680}^+)$. (vi) $E_m(Pheo^-/Pheo)$ has been indirectly measured in spinach [−410 mV (202), −420 mV (201)] or *Synechocystis* 6803 [−440 mV (198)] with reference to an $E_m(Q_A^-/Q_A)$ value of −80 mV (199, 200), and directly measured by spectroelectrochemistry in *Thermosynechococcus elongatus* containing D1:1-PSII [−522 mV (44)] or D1:2-PSII [−508 mV (128)]. (vii) $E_m(Q_A^-/Q_A)$ was directly measured by redox titrations in spinach [−80 mV (200)] and *Scenedesmus obliquus* [−80 mV (199)], and by spectroelectrochemistry in *T. elongatus* containing D1:1-PSII (−124 mV) or D1:2 (−83 mV) (130), *Chlamydomonas reinhardtii* (−162 mV), spinach (−149 mV), and *Cyanidioschyzon merolae* (−92 mV) (129). (viii) $E_m(Q_B^-/Q_B)$ was indirectly measured in pea chloroplasts [$E_m(Q_A^-/Q_A) - E_m(Q_B^-/Q_B) = -70$ mV (135)] or *Synechocystis* 6803 [$E_m(Q_A^-/Q_A) - E_m(Q_B^-/Q_B) = -83$ mV (203)].

to the intrinsic turnover rate per PSII from a knowledge of the Chl concentration per RC. This conversion is also given in **Table 2** and reveals that the light-saturated rate using artificial electron acceptors is remarkably similar for PSIIs from many different organisms, ranging from 27 to 67 O_2 s^{-1} $PSII^{-1}$. To the best of our knowledge, the highest sustained rate measured in vitro is 67 s^{-1} in the thermophilic cyanobacterium *Thermosynechococcus elongatus* (157). The use of artificial electron acceptors with their inefficient reoxidation rate is commonly believed to limit PSII turnover in vitro. As previously described, the Kok cycle operates at less than 1–2 ms per turnover in dark-adapted (resting) enzyme. Thus, the maximal single turnover rate of PSII should be 500–1,000 s^{-1}. Indeed, instantaneous O_2 release as measured by polarography (121, 122), EPR (123), or photoacoustics (124) occurs in 1.2–2.2 ms

Table 2 Light-saturated PSII turnover frequency in vitro (O_2 evolution) and in vivo (variable Chl *a* fluorescence)

Species	Preparation	Turnover frequency (s^{-1})
Spinacia oleracea	Membrane fragments	30[a]
Chlamydomonas reinhardtii	Membrane fragments	45[b]
Chlamydomonas reinhardtii	Core complexes	27[c]
Thermosynechococcus elongatus	Core complexes	67[d]
Synechocystis sp. PCC 6803	Core complexes	27[e]
Synechocystis sp. PCC 6803	Core complexes	35[f]
Synechocystis sp. PCC 6803	Core complexes	25[g]
Chlorella pyrenoidosa	Whole cells	25[h]
Arthrospira maxima	Whole cells	88[h]

Unless otherwise specified, all data refer to a temperature range of 20–25°C. Abbreviations: Chl, chlorophyll; PSII, photosystem II.
[a]BBY preparation (25), 450 μmol O_2 (mg Chl)$^{-1}$ h^{-1}, 270 Chl/$Y_D^{\bullet}$ (181).
[b]PSII-enriched thylakoid membrane fragments, 650 μmol O_2 (mg Chl)$^{-1}$ h^{-1}, 276 Chl/4 Mn (28).
[c]His-tag-labeled D2 subunit, 2400 μmol O_2 (mg Chl)$^{-1}$ h^{-1}, 46 Chl/ $Y_D^{\bullet}$ (182).
[d]His-tag-labeled CP43 subunit, 6000 μmol O_2 (mg Chl)$^{-1}$ h^{-1}, 45 Chl/ $Y_D^{\bullet}$ (44, 157) at 45°C.
[e]2500 μmol O_2 (mg Chl)$^{-1}$ h^{-1}, 44 Chl/0.25 O_2 (183).
[f]2400 μmol O_2 (mg Chl)$^{-1}$ h^{-1}, 59 Chl/ $Y_D^{\bullet}$ (184).
[g]His-tag-labeled CP47 subunit, 2440 μmol O_2 (mg Chl)$^{-1}$ h^{-1}, 41 Chl/cyt b_{559} (185).
[h]Values correspond to turnover frequency at one-half maximum *Q* value (21).

(see **Table 1**), corresponding to rates of 455–833 s^{-1}.

In vivo, PSII turnover kinetics are readily measured by monitoring variable Chl *a* fluorescence using fast repetition rate fluorometry (21, 158). The damping rate for the amplitude of period-four oscillations of variable Chl *a* fluorescence (F_v) reflects the intrinsic turnover kinetics of the PSII-WOC (**Figure 2*b***). Two analytical approaches are used (21). Fourier analysis of these oscillations gives the period of the oscillations directly and provides a model-independent measure of the dissipation of the catalytic cycle with flashing rate (**Figure 2*c***). Alternatively, the amplitude of the oscillations can be mathematically fit to the classic (19, 20) or extended (159) Kok model (**Figure 2*a***) to estimate the probability of a miss (α) or double hit (β). The Kok parameters are then used to calculate a familiar quantity in resonator theory called the quality factor of the cycle, $Q = (\alpha + \beta)^{-1}$. When *Q* drops to half its peak value, the power entering the Kok cycle drops by half. As shown in **Figure 7**, the in vivo upper limit of WOC turnover rate varies considerably by species. The WOC cycling efficiency of the green alga *Chlorella pyrenoidosa* sharply decreases above STF frequencies greater than 25 s^{-1} and reaches 50% at 100 s^{-1}. Because four flashes are required for one WOC cycle,

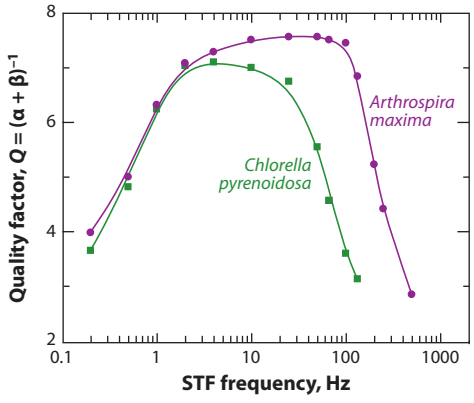

Figure 7

Dependence of period-four oscillations in F_v/F_m on the dark time between single-turnover flashes (STFs) for intact cells of the green alga *Chlorella pyrenoidosa* (*green*) and the cyanobacterium *Arthrospira maxima* (*purple*). The quality factor values, $Q = (\alpha + \beta)^{-1}$, were obtained by fits to a standard two-parameter Kok model (see **Figure 2*a***). The figure is based on raw data from Reference 21.

the turnover frequency can be estimated as 1/4 × 100 s^{-1} = 25 s^{-1}. The fastest in vivo water splitter is the hypercarbonate cyanobacterium *Arthrospira maxima*. The WOC cycling efficiency decreases above STF frequencies greater than 100 s^{-1}, dropping to 50% at 350 s^{-1} (turnover rate = 88 s^{-1}) (21). This drop-off in rate was limited by the buffer capacity of the lumen and thus attributed to proton release kinetics (92). In vivo PSII turnover efficiency is strongly affected by the redox state of the PQ pool, which is controlled by downstream electron carriers (including cyt b_6f, PSI, and alternative oxidases) (29).

SUMMARY POINTS

1. The greatly improved resolution of the PSII-WOC atomic structure (O atom chemical specification and coordination revealed) enables a structure-based assignment of the chemical bonding between Mn and O and gives the location of many water molecules.
2. The PSII reaction center core is remarkably conserved across cyanobacteria, algae, and higher plants, but significant differences in low-molecular-weight and extrinsic subunits exist.
3. New information identifying the oxidation states of the Mn atoms in the WOC has come from spectroscopic, computation, and photoassembly studies and indicates discrepancies that are still under debate.
4. Consideration of the improved atomic structure and oxidation states data, together with numerous other studies, has provided new insights that enable formation of likely chemical mechanisms of water oxidation and substrate water exchange.
5. Short-circuiting electron transfer pathways occur within PSII that lower the efficiency of WOC cycling while serving roles in photoprotection.
6. The PSII-WOCs from plants, algae, and cyanobacteria operate at light-saturated rates that are remarkably consistent in vitro and in vivo (25–88 s^{-1}).

FUTURE ISSUES

1. Can a high-resolution XRD structure of a green algal or plant PSII be obtained? How would it differ from the thermophilic cyanobacterial structures?
2. Can high-resolution XRD structures of S_0, S_2, S_3, and S_4 be obtained?
3. What spectroscopic, computational, and reconstitution experiments are needed for the field to arrive at a consensus mechanism for WOC turnover?
4. Can the efficiency of PSII turnover in vivo be improved from less than 100 s^{-1} to approach the intrinsic WOC turnover limit of 500–1,000 s^{-1}?
5. What additional principles can our current understanding of PSII offer to scientists designing more efficient abiotic catalysts using Earth-abundant materials?

DISCLOSURE STATEMENT

The authors are not aware of any affiliations, memberships, funding, or financial holdings that might be perceived as affecting the objectivity of this review.

ACKNOWLEDGMENTS

The authors are supported by the Division of Chemical Sciences, Geosciences, and Biosciences, Office of Basic Energy Sciences of the U.S. Department of Energy (Grant DE-FG02-10ER16195). D.J.V. is supported by the Department of Defense, Army Research Office, through a National Defense Science and Engineering Graduate Fellowship (32CFR168a) and a National Science Foundation Graduate Research Fellowship (DGE-0937373). We thank Drs. Clyde Cady, Nick Cox, Ron Pace, Tom Umile, Leslie Vogt, and Chase Zachary for helpful discussions.

LITERATURE CITED

1. Falkowski PG, Raven JA. 2007. *Aquatic Photosynthesis*. Princeton, NJ: Princeton Univ. Press. 500 pp. 2nd ed.
2. Dismukes GC, Blankenship RE. 2005. The origin and evolution of photosynthetic oxygen production. See Ref. 204, pp. 683–95.
3. Blankenship RE, Tiede DM, Barber J, Brudvig GW, Fleming G, et al. 2011. Comparing photosynthetic and photovoltaic efficiencies and recognizing the potential for improvement. *Science* 332:805–9
4. Dau H, Zaharieva I. 2009. Principles, efficiency, and blueprint character of solar-energy conversion in photosynthetic water oxidation. *Acc. Chem. Res.* 42:1861–70
5. Hambourger M, Moore GF, Kramer DM, Gust D, Moore AL, Moore TA. 2009. Biology and technology for photochemical fuel production. *Chem. Soc. Rev.* 38:25–35
6. Dismukes GC, Brimblecombe R, Felton GAN, Pryadun RS, Sheats JE, et al. 2009. Development of bioinspired Mn_4O_4-cubane water oxidation catalysts: lessons from photosynthesis. *Acc. Chem. Res.* 42:1935–43
7. Björn L, Papageorgiou G, Blankenship RE, Govindjee. 2009. A viewpoint: why chlorophyll-*a*? *Photosynth. Res.* 99:85–98
8. Chen M, Schliep M, Willows RD, Cai Z-L, Neilan BA, Scheer H. 2010. A red-shifted chlorophyll. *Science* 329:1318–19
9. Manning WM, Strain HH. 1943. Chlorophyll d, a green pigment of red algae. *J. Biol. Chem.* 151:1–19
10. Porra RJ, Thompson WA, Kriedemann PE. 1989. Determination of accurate extinction coefficients and simultaneous equations for assaying chlorophylls *a* and *b* extracted with four different solvents: verification of the concentration of chlorophyll standards by atomic absorption spectroscopy. *Biochim. Biophys. Acta* 975:384–94
11. Li Y, Scales N, Blankenship RE, Willows RD, Chen M. 2012. Extinction coefficient for red-shifted chlorophylls: Chlorophyll *d* and chlorophyll *f*. *Biochim. Biophys. Acta* 1817:1292–98
12. Dasgupta J, Ananyev GM, Dismukes GC. 2008. Photoassembly of the water-oxidizing complex in photosystem II. *Coord. Chem. Rev.* 252:347–60
13. Renger G, Renger T. 2008. Photosystem II: the machinery of photosynthetic water splitting. *Photosynth. Res.* 98:53–80
14. Barber J. 2008. Crystal structure of the oxygen-evolving complex of photosystem II. *Inorg. Chem.* 47:1700–10
15. Ferreira K, Iverson T, Maghlaoui K, Barber J, Iwata S. 2004. Architecture of the photosynthetic oxygen-evolving center. *Science* 303:1831–38
16. Guskov A, Kern J, Gabdulkhakov A, Broser M, Zouni A, Saenger W. 2009. Cyanobacterial photosystem II at 2.9-Å resolution and the role of quinones, lipids, channels and chloride. *Nat. Struct. Mol. Biol.* 16:334–42
17. Umena Y, Kawakami K, Shen J-R, Kamiya N. 2011. Crystal structure of oxygen-evolving photosystem II at a resolution of 1.9 Å. *Nature* 473:55–60
18. Joliot P, Barbieri G, Chabaud R. 1969. Un nouveau modele des centres photochimiques du systeme II. *Photochem. Photobiol.* 10:309–29
19. Kok B, Forbush B, McGloin M. 1970. Cooperation of charges in photosynthetic O_2 evolution-I. A linear four step mechanism. *Photochem. Photobiol.* 11:457–75
20. Forbush B, Kok B, McGloin MP. 1971. Cooperation of charges in photosynthetic O_2 evolution-II. Damping of flash yield oscillation, deactivation. *Photochem. Photobiol.* 14:307–21

21. Ananyev G, Dismukes GC. 2005. How fast can photosystem II split water? Kinetic performance at high and low frequencies. *Photosynth. Res.* 84:355–65
22. Shi L-X, Schroder WP. 2004. The low molecular mass subunits of the photosynthetic supracomplex, photosystem II. *Biochim. Biophys. Acta* 1608:75–96
23. Shi LX, Hall M, Funk C, Schroder WP. 2012. Photosystem II, a growing complex: updates on newly discovered components and low molecular mass proteins. *Biochim. Biophys. Acta* 1817:13–25
24. Thorton L, Roose JL, Pakrasi HB, Ikeuchi M. 2005. The low molecular weight proteins of photosystem II. See Ref. 204, pp. 121–37
25. Berthold DA, Babcock GT, Yocum CF. 1981. A highly resolved, oxygen-evolving photosystem II preparation from spinach thylakoid membranes. *FEBS Lett.* 134:231–34
26. Boekema EJ, Hankamer B, Bald D, Kruip J, Nield J, et al. 1995. Supramolecular structure of the photosystem II complex from green plants and cyanobacteria. *Proc. Natl. Acad. Sci. USA* 92:175–79
27. Dekker JP, Boekema EJ. 2005. Supramolecular organization of thylakoid membrane proteins in green plants. *Biochim. Biophys. Acta* 1706:12–39
28. Shim H, Cao J, Govindjee G, Debrunner PG. 1990. Purification of highly active oxygen-evolving photosystem II from *Chlamydomonas reinhardtii*. *Photosynth. Res.* 26:223–28
29. Kramer D, Evans J. 2011. The importance of energy balance in improving photosynthetic productivity. *Plant Physiol.* 155:70–78
30. Nakamura Y, Kaneko T, Sato S, Mimuro M, Miyashita H, et al. 2003. Complete genome structure of *Gloeobacter violaceus* PCC 7421, a cyanobacterium that lacks thylakoids. *DNA Res.* 10:137–45
31. Bricker TM, Roose JL, Fagerlund RD, Frankel LK, Eaton-Rye JJ. 2012. The extrinsic proteins of photosystem II. *Biochim. Biophys. Acta* 1817:121–42
32. Roose J, Wegener K, Pakrasi H. 2007. The extrinsic proteins of photosystem II. *Photosynth. Res.* 92:369–87
33. Shen J-R, Inoue Y. 1993. Binding and functional properties of two new extrinsic components, cytochrome *c*-550 and a 12-kDa protein, in cyanobacterial photosystem II. *Biochemistry* 32:1825–32
34. Han K-C, Shen J-R, Ikeuchi M, Inoue Y. 1994. Chemical crosslinking studies of extrinsic proteins in cyanobacterial photosystem II. *FEBS Lett.* 355:121–24
35. Shen J-R, Qian M, Inoue Y, Burnap RL. 1998. Functional characterization of *Synechocystis* sp. PCC 6803 Δ*psb*U and Δ*psb*V mutants reveals important roles of cytochrome *c*-550 in cyanobacterial oxygen evolution. *Biochemistry* 37:1551–58
36. Katoh H, Itoh S, Shen J-R, Ikeuchi M. 2001. Functional analysis of *psb*V and a novel c-type cytochrome gene *psbV2* of the thermophilic cyanobacterium *Thermosynechococcus elongatus* strain BP-1. *Plant Cell Physiol.* 42:599–607
37. Nishiyama Y, Hayashi H, Watanabe T, Murata N. 1994. Photosynthetic oxygen evolution is stabilized by cytochrome c_{550} against heat inactivation in *Synechococcus* sp. PCC 7002. *Plant Physiol.* 105:1313–19
38. Li Z, Andrews H, Eaton-Rye JJ, Burnap RL. 2004. In situ effects of mutations of the extrinsic cytochrome c_{550} of photosystem II in *Synechocystis* sp. PCC6803. *Biochemistry* 43:14161–70
39. Roncel M, Kirilovsky D, Guerrero F, Serrano A, Ortega JM. 2012. Photosynthetic cytochrome *c*550. *Biochim. Biophys. Acta* 1817:1152–63
40. Mulo P, Sicora C, Aro E-M. 2009. Cyanobacterial *psbA* gene family: optimization of oxygenic photosynthesis. *Cell. Mol. Life Sci.* 66:3697–710
41. Golden SS. 1995. Light-responsive gene expression in cyanobacteria. *J. Bacteriol.* 177:1651–54
42. Sander J, Nowaczyk M, Buchta J, Dau H, Vass I, et al. 2010. Functional characterization and quantification of the alternative *psbA* copies in *Thermosynechococcus elongatus* and their role in photoprotection. *J. Biol. Chem.* 285:29851–56
43. Sane PV, Ivanov AG, Sveshnikov D, Huner NPA, Oquist G. 2002. A transient exchange of the photosystem II reaction center protein D1:1 with D1:2 during low temperature stress of *Synechococcus* sp. PCC 7942 in the light lowers the redox potential of Q_B. *J. Biol. Chem.* 277:32739–45
44. Sugiura M, Kato Y, Takahashi R, Suzuki H, Watanabe T, et al. 2010. Energetics in photosystem II from *Thermosynechococcus elongatus* with a D1 protein encoded by either the *psbA1* or *psbA3* gene. *Biochim. Biophys. Acta* 1797:1491–99

45. Vinyard D, Gimpel G, Ananyev G, Cornejo M, Golden SS, et al. 2013. Natural variants of photosystem II subunit D1 tune photochemical fitness to solar intensity. *J. Biol. Chem.* 288:5451–62
46. Summerfield TC, Toepel J, Sherman LA. 2008. Low-oxygen induction of normally cryptic *psbA* genes in cyanobacteria. *Biochemistry* 47:12939–41
47. Sicora CI, Ho FM, Salminen T, Styring S, Aro E-M. 2009. Transcription of a "silent" cyanobacterial *psbA* gene is induced by microaerobic conditions. *Biochim. Biophys. Acta* 1787:105–12
48. Dasgupta J, van Willigen RT, Dismukes GC. 2004. Consequences of structural and biophysical studies for the molecular mechanism of photosynthetic oxygen evolution: functional roles for calcium and bicarbonate. *Phys. Chem. Chem. Phys.* 6:4793–802
49. Peloquin JM, Campbell KA, Randall DW, Evanchik MA, Pecoraro VL, et al. 2000. ^{55}Mn ENDOR of the S_2-state multiline EPR signal of photosystem II: implications on the structure of the tetranuclear Mn cluster. *J. Am. Chem. Soc.* 122:10926–42
50. Dismukes GC, Zheng M, Hutchins R, Philo J. 1994. The inorganic biochemistry of photosynthetic water oxidation. *Biochem. Soc. Trans.* 22:323–27
51. Bernadou J, Meunier B. 1998. 'Oxo-hydroxo tautomerism' as useful mechanistic tool in oxygenation reactions catalysed by water-soluble metalloporphyrins. *Chem. Commun.* 20:2167–73
52. Meunier B, Bernadou J. 2002. Metal-oxo species in P450 enzymes and biomimetic models. Oxo-hydroxo tautomerism with water-soluble metalloporphyrins. *Top. Catal.* 21:47–54
53. Yano J, Kern J, Sauer K, Latimer MJ, Pushkar Y, et al. 2006. Where water is oxidized to dioxygen: structure of the photosynthetic Mn_4Ca cluster. *Science* 314:821–25
54. Yano J, Yachandra VK. 2008. Where water is oxidized to dioxygen: structure of the photosynthetic Mn_4Ca cluster from X-ray spectroscopy. *Inorg. Chem.* 47:1711–26
55. Dau H, Grundmeier A, Loja P, Haumann M. 2008. On the structure of the manganese complex of photosystem II: extended-range EXAFS data and specific atomic-resolution models for four S-states. *Philos. Trans. R. Soc. Lond. Ser. B* 363:1237–44
56. Siegbahn PEM. 2008. A structure-consistent mechanism for dioxygen formation in photosystem II. *Chem. Eur. J.* 14:8290–302
57. Siegbahn PEM. 2009. Structures and energetics for O_2 formation in photosystem II. *Acc. Chem. Res.* 42:1871–80
58. Petrie S, Gatt P, Stranger R, Pace RJ. 2012. Modelling the metal atom positions of the photosystem II water oxidising complex: a density functional theory appraisal of the 1.9 Å resolution crystal structure. *Phys. Chem. Chem. Phys.* 14:11333–43
59. Visser H, Anxolabehere-Mallart E, Bergmann U, Glatzel P, Robblee JH, et al. 2001. Mn K-edge XANES and Kβ XES studies of two Mn-oxo binuclear complexes: investigation of three different oxidation states relevant to the oxygen-evolving complex of photosystem II. *J. Am. Chem. Soc.* 123:7031–39
60. Yano J, Kern J, Irrgang K-D, Latimer MJ, Bergmann U, et al. 2005. X-ray damage to the Mn_4Ca complex in single crystals of photosystem II: a case study for metalloprotein crystallography. *Proc. Natl. Acad. Sci. USA* 102:12047–52
61. Grabolle M, Haumann M, Müller C, Liebisch P, Dau H. 2006. Rapid loss of structural motifs in the manganese complex of oxygenic photosynthesis by X-ray irradiation at 10–300 K. *J. Biol. Chem.* 281:4580–88
62. Dau H, Liebisch P, Haumann M. 2004. The structure of the manganese complex of photosystem II in its dark-stable S_1-state-EXAFS results in relation to recent crystallographic data. *Phys. Chem. Chem. Phys.* 6:4781–92
63. Haumann M, Liebisch P, Muller C, Barra M, Grabolle M, Dau M. 2005. Photosynthetic O_2 formation tracked by time-resolved X-ray experiments. *Science* 310:1019–21
64. Ames W, Pantazis DA, Krewald V, Cox N, Messinger J, et al. 2011. Theoretical evaluation of structural models of the S_2 state in the oxygen evolving complex of photosystem II: protonation states and magnetic interactions. *J. Am. Chem. Soc.* 133:19743–57
65. Grundmeier A, Dau H. 2012. Structural models of the manganese complex of photosystem II and mechanistic implications. *Biochim. Biophys. Acta* 1817:88–105
66. Luber S, Rivalta I, Umena Y, Kawakami K, Shen J-R, et al. 2011. S_1-state model of the O_2-evolving complex of photosystem II. *Biochemistry* 50:6308–11

67. Siegbahn PEM. 2011. The effect of backbone constraints: the case of water oxidation by the oxygen-evolving complex in PSII. *ChemPhysChem* 12:3274–80
68. Frasch W, Sayre RT. 2001. Remembering George Cheniae. *Photosynth. Res.* 70:245–47
69. Tamura N, Cheniae GM. 1986. Requirements for the photoligation of Mn^{2+} in PSII membranes and the expression of water-oxidizing activity of the polynuclear Mn-catalyst. *FEBS Lett.* 200:231–36
70. Baranov SV, Tyryshkin AM, Katz D, Dismukes GC, Ananyev G, Klimov VV. 2004. Bicarbonate is a native cofactor for assembly of the manganese cluster of the photosynthetic water oxidizing complex. Kinetics of reconstitution of oxygen evolution by photoactivation. *Biochemistry* 43:2070–79
71. Ananyev G, Nguyen T, Putnam-Evans C. 2005. Mutagenesis of CP43-arginine-357 to serine reveals new evidence for (bi)carbonate functioning in the water oxidizing complex of photosystem II. *Photochem. Photobiol. Sci.* 4:991–98
72. Cheniae GM, Martin IF. 1971. Photoactivation of manganese catalyst of O_2 evolution. 1. Biochemical and kinetic aspects. *Biochim. Biophys. Acta* 253:167–81
73. Radmer R, Cheniae GM. 1971. Photoactivation of the manganese catalyst of O_2 evolution II. A two-quantum mechanism. *Biochim. Biophys. Acta* 253:182–86
74. Tamura N, Cheniae GM. 1987. Photoactivation of the water-oxidizing complex in photosystem II membranes depleted of Mn and extrinsic proteins. I. Biochemical and kinetic characterization. *Biochim. Biophys. Acta* 890:179–94
75. Ananyev GM, Zaltsman L, Vasko C, Dismukes GC. 2001. The inorganic biochemistry of photosynthetic oxygen evolution/water oxidation. *Biochim. Biophys. Acta* 1503:52–68
76. Dismukes GC, Ananyev GM, Watt R. 2005. Photo-assembly of the catalytic managanese cluster. See Ref. 204, pp. 609–26
77. Burnap RL. 2004. D1 protein processing and Mn cluster assembly in light of the emerging photosystem II structure. *Phys. Chem. Chem. Phys.* 6:4803–9
78. Miller A-F, Brudvig G. 1989. Manganese and calcium requirement for reconstruction of oxygen-evolution activity in manganese-depleted photosystem II membranes. *Biochemistry* 28:8181–90
79. Zaltsman L, Ananyev G, Bruntrager E, Dismukes GC. 1997. Quantitative kinetic model for photoassembly of the photosynthetic water oxidase from its inorganic constituents: requirements for manganese and calcium in the kinetically resolved steps. *Biochemistry* 36:8914–22
80. Baranov SV, Ananyev G, Klimov VV, Dismukes GC. 2000. Bicarbonate accelerates assembly of the inorganic core of the water-oxidizing complex in manganese-depleted photosystem II: a proposed biogeochemical role for atmospheric carbon dioxide in oxygen photosynthesis. *Biochemistry* 39:6060–65
81. Ananyev GM, Murphy A, Abe Y, Dismukes GC. 1999. Remarkable affinity and selectivity for Cs^+ and uranyl (UO_2^{2+}) binding to the manganese site of the apo-water oxidation complex of photosystem II. *Biochemistry* 38:7200–9
82. Tyryshkin AM, Watt RK, Baranov SV, Dasgupta J, Hendrich MP, Dismukes GC. 2006. Spectroscopic evidence for Ca^{2+} involvement in the assembly of the Mn_4Ca cluster in the photosynthetic water-oxidizing complex. *Biochemistry* 45:12876–89
83. Dasgupta J, Tyryshkin A, Baranov S, Dismukes G. 2010. Bicarbonate coordinates to Mn^{3+} during photo-assembly of the catalytic Mn_4Ca core of photosynthetic water oxidation: EPR characterization. *Appl. Magn. Reson.* 37:137–50
84. Hwang HJ, Burnap RL. 2005. Multiflash experiments reveal a new kinetic phase of photosystem II manganese cluster assembly in *Synechocystis* sp. PCC 6803 in vivo. *Biochemistry* 44:9766–74
85. Bartlett JE, Baranov SV, Ananyev GM, Dismukes GC. 2008. Calcium controls the assembly of the photosynthetic water-oxidizing complex: a cadmium(II) inorganic mutant of the Mn_4Ca core. *Philos. Trans. R. Soc. Lond. Ser. B* 363:1253–61
86. Kolling D, Cox N, Ananyev G, Pace RJ, Dismukes GC. 2012. What are the oxidation states of manganese required to catalyze photosynthetic water oxidation? *Biophys. J.* 103:313–22
87. Chen C, Kazimir J, Cheniae GM. 1995. Calcium modulates the photo-assembly of photosystem II Mn_4-clusters by preventing ligation of nonfunctional high-valency states of manganese. *Biochemistry* 34:13511–26

88. Campbell KA, Force DA, Nixon PJ, Dole F, Diner BA, Britt RD. 2000. Dual-mode EPR detects the initial intermediate in photoassembly of the photosystem II Mn cluster: the influence of amino acid residue 170 of the D1 polypeptide on Mn coordination. *J. Am. Chem. Soc.* 122:3754–61
89. Pokhrel R, McConnell IL, Brudvig GW. 2011. Chloride regulation of enzyme turnover: application to the role of chloride in photosystem II. *Biochemistry* 50:2725–34
90. Dasgupta J, Tyryshkin AM, Dismukes GC. 2007. ESEEM spectroscopy reveals carbonate and a N-donor protein-ligand binding to Mn^{2+} in the photoassembly reaction of the Mn_4Ca cluster in photosystem II. *Angew. Chem. Int. Ed.* 46:8028–31
91. Shevela D, Eaton-Rye JJ, Shen J-R, Govindjee. 2012. Photosystem II and the unique role of bicarbonate: a historical perspective. *Biochim. Biophys. Acta* 1817:1134–51
92. Carrieri D, Ananyev G, Brown T, Dismukes GC. 2007. In vivo bicarbonate requirement for water oxidation by photosystem II in the hypercarbonate-requiring cyanobacterium *Arthrospira maxima*. *J. Inorg. Biochem.* 101:1865–74
93. Bersuker IB. 1996. *Electronic Structure and Properties of Transition Metal Compounds: Introduction to the Theory*. New York: John Wiley & Sons
94. Richens DT. 1997. *The Chemistry of Aqua Ions*. Chichester, UK: John Wiley & Sons
95. Hillier W, Wydrzynski T. 2008. ^{18}O-water exchange in photosystem II: Substrate binding and intermediates of the water splitting cycle. *Coord. Chem. Rev.* 252:306–17
96. Gatt P, Petrie S, Stranger R, Pace RJ. 2012. Rationalizing the 1.9 Å crystal structure of photosystem II—a remarkable Jahn-Teller balancing act induced by a single proton transfer. *Angew. Chem. Int. Ed.* 51:12025–28
97. Wu J-Z, Sellitto E, Yap GPA, Sheats J, Dismukes GC. 2004. Trapping an elusive intermediate in manganese-oxo cubane chemistry. *Inorg. Chem.* 43:5795–97
98. Dau H, Haumann M. 2007. Eight steps preceding O-O bond formation in oxygenic photosynthesis—a basic reaction cycle of the photosystem II manganese complex. *Biochim. Biophys. Acta* 1767:472–83
99. Czernuszewicz RS, Su YO, Stern MK, Macor KA, Kim D, et al. 1988. Oxomanganese(IV) porphyrins identified by resonance Raman and infrared spectroscopy. Weak bonds and the stability of the half-filled t_{2g} subshell. *J. Am. Chem. Soc.* 110:4158–65
100. Lee DG, Moylan CR, Hayashi T, Brauman JI. 1987. Photochemistry of aqueous permanganate ion. *J. Am. Chem. Soc.* 109:3003–10
101. Nakai H, Ohmori Y, Nakatsuji H. 1995. Theoretical study on the photochemical decomposition reaction of permanganate ion, MnO_4^-. *J. Phys. Chem.* 99:8550–55
102. Siegbahn PEM. 2011. Recent theoretical studies of water oxidation in photosystem II. *J. Photochem. Photobiol. B.* 104:94–99
103. McEvoy JP, Brudvig GW. 2006. Water-splitting chemistry of photosystem II. *Chem. Rev.* 106:4455–83
104. Rapatskiy L, Cox N, Savitsky A, Ames WM, Sander J, et al. 2012. Detection of the water-binding sites of the oxygen-evolving complex of photosystem II using W-band ^{17}O electron–electron double resonance-detected NMR spectroscopy. *J. Am. Chem. Soc.* 134:16619–34
105. Krishtalik LI. 1986. Energetics of multielectron reactions. Photosynthetic oxygen evolution. *Biochim. Biophys. Acta* 849:162–71
106. Krishtalik LI. 1990. Activation energy of photosynthetic oxygen evolution: an attempt at theoretical analysis. *Bioelectrochem. Bioenerget.* 23:249–63
107. Styring S, Sjoholm J, Mamedov F. 2012. Two tyrosines that changed the world: interfacing the oxidizing power of photochemistry to water splitting in photosystem II. *Biochim. Biophys. Acta* 1817:76–87
108. Berry BW, Martinez-Rivera MC, Tommos C. 2012. Reversible voltammograms and a Pourbaix diagram for a protein tyrosine radical. *Proc. Natl. Acad. Sci. USA* 109:9739–43
109. Deak Z, Vass I, Strying S. 1994. Redox interaction of tyrosine-D with the S-states of the water-oxidizing complex in intact and chloride-depleted photosystem II. *Biochim. Biophys. Acta* 1185:65–74
110. Styring S, Rutherford AW. 1987. In the oxygen-evolving complex of photosystem II the S_0 state is oxidized to the S_1 state by D^+ (signal II_{slow}). *Biochemistry* 26:2401–5
111. Vass I, Styring S. 1991. pH-Dependent charge equilibria between tyrosine-D and the S states in photosystem II. Estimation of relative midpoint redox potentials. *Biochemistry* 30:830–39

112. Renger G. 1983. Biological energy conservation. In *Biophysics*, ed. W Hoppe, W Lohmann, H Markl, H Ziegler, pp. 347–71. Berlin: Springer
113. Brettel K, Schlodder E, Witt HT. 1984. Nanosecond reduction kinetics of photooxidized chlorophyll-a_{II} (P680) in single flashes as a probe for the electron pathway, H^+-release and charge accumulation in the O_2-evolving complex. *Biochim. Biophys. Acta* 766:403–15
114. Eckert HJ, Renger G. 1988. Temperature dependence of $P680^+$ reduction in O_2-evolving PS II membrane fragments at different redox states S_i of the water oxidizing system. *FEBS Lett.* 236:425–31
115. Karge M, Irrgang KD, Sellin S, Feinaugle R, Liu B, et al. 1996. Effects of hydrogen/deuterium exchange on photosynthetic water cleavage in PS II core complexes from spinach. *FEBS Lett.* 378:140–44
116. Kuhn P, Pieper J, Kaminskaya O, Eckert HJ, Lechner RE, et al. 2005. Reaction pattern of photosystem II: oxidative water cleavage and protein flexibility. *Photosynth. Res.* 84:317–23
117. Babcock GT, Blankenship RE, Sauer K. 1976. Reaction kinetics for positive charge accumulation on the water side of chloroplast photosystem II. *FEBS Lett.* 61:286–89
118. Razeghifard MR, Pace RJ. 1997. Electron paramagnetic resonance kinetic studies of the S states in spinach PSII membranes. *Biochim. Biophys. Acta* 1322:141–50
119. Rappaport F, Blancharddesce M, Lavergne J. 1994. Kinetics of electron-transfer and electrochromic change during the redox transitions of the photosynthetic oxygen-evolving complex. *Biochim. Biophys. Acta* 1184:178–92
120. Noguchi T, Suzuki H, Tsuno M, Sugiura M, Kato C. 2012. Time-resolved infrared detection of the proton and protein dynamics during photosynthetic oxygen evolution. *Biochemistry* 51:3205–14
121. Bouges-Bocquet B. 1973. Limiting steps in photosystem II and water decomposition in *Chlorella* and spinach chloroplasts. *Biochim. Biophys. Acta* 292:772–85
122. Etienne AL. 1968. [Study of the thermic stage of photosynthetic emission of oxygen by a discharge method]. *Biochim. Biophys. Acta* 153:895–97
123. Tang X-S, Moussavi M, Dismukes GC. 1991. Monitoring oxygen concentration in solution by ESR oximetry using lithium phthalocyanine: application in photosynthesis. *J. Am. Chem. Soc.* 113:5914–15
124. Canaani O, Malkin S, Mauzerall D. 1988. Pulsed photoacoustic detection of flash-induced oxygen evolution from intact leaves and its oscillations. *Proc. Natl. Acad. Sci. USA* 85:4725–29
125. Kolling DRJ, Brown TS, Ananyev G, Dismukes GC. 2009. Photosynthetic oxygen evolution is not reversed at high oxygen pressures: mechanistic consequences for the water-oxidizing complex. *Biochemistry* 48:1381–89
126. Shevela D, Beckmann K, Clausen J, Junge W, Messinger J. 2011. Membrane-inlet mass spectrometry reveals a high driving force for oxygen production by photosystem II. *Proc. Natl. Acad. Sci. USA* 108:3602–7
127. Merry SAP, Nixon PJ, Barter LMC, Schilstra M, Porter G, et al. 1998. Modulation of quantum yield of primary radical pair formation in photosystem II by site-directed mutagenesis affecting radical cations and anions. *Biochemistry* 37:17439–47
128. Kato Y, Sugiura M, Oda A, Watanabe T. 2009. Spectroelectrochemical determination of the redox potential of pheophytin a, the primary electron acceptor in photosystem II. *Proc. Natl. Acad. Sci. USA* 106:17365–70
129. Shibamoto T, Kato Y, Nagao R, Yamazaki T, Tomo T, Watanabe T. 2010. Species-dependence of the redox potential of the primary quinone electron acceptor Q_A in photosystem II verified by spectroelectrochemistry. *FEBS Lett.* 584:1526–30
130. Kato Y, Shibamoto T, Yamamoto S, Watanabe T, Ishida N, et al. 2012. Influence of the PsbA1/PsbA3, Ca^{2+}/Sr^{2+} and Cl^-/Br^- exchanges on the redox potential of the primary quinone Q_A in photosystem II from *Thermosynechococcus elongatus* as revealed by spectroelectrochemistry. *Biochim. Biophys. Acta* 1817:1998–2004
131. Shibamoto T, Kato Y, Sugiura M, Watanabe T. 2009. Redox potential of the primary plastoquinone electron acceptor Q_A in photosystem II from *Thermosynechococcus elongatus* determined by spectroelectrochemistry. *Biochemistry* 48:10682–84
132. Krieger-Liszkay A, Rutherford AW. 1998. Influence of herbicide binding on the redox potential of the quinone acceptor in photosystem II: relevance to photodamage and phytotoxicity. *Biochemistry* 37:17339–44

133. Ishikita H, Knapp E-W. 2005. Control of quinone redox potentials in photosystem II: electron transfer and photoprotection. *J. Am. Chem. Soc.* 127:14714–20
134. de Wijn R, van Gorkom HJ. 2001. Kinetics of electron transfer from Q_A to Q_B in photosystem II. *Biochemistry* 40:11912–22
135. Robinson HH, Crofts AR. 1983. Kinetics of the oxidation-reduction reactions of the photosystem II quinone acceptor complex, and the pathway for deactivation. *FEBS Lett.* 153:221–26
136. Weiss W, Renger G. 1984. UV-spectral characterization in Tris-washed chloroplasts of the redox component D_1 which functionally connects the reaction center with the water-oxidizing enzyme system Y in photosynthesis. *FEBS Lett.* 169:219–23
137. Bowes J, Crofts AR, Arntzen CJ. 1980. Redox reactions on the reducing side of photosystem II in chloroplasts with altered herbicide binding properties. *Arch. Biochem. Biophys.* 200:303–8
138. Shinopoulos KE, Brudvig GW. 2012. Cytochrome b_{559} and cyclic electron transfer within photosystem II. *Biochim. Biophys. Acta* 1817:66–75
139. Babcock GT, Sauer K. 1973. Electron paramagnetic resonance signal II in spinach chloroplasts. I. Kinetic analysis for untreated chloroplasts. *Biochim. Biophys. Acta* 325:483–503
140. Magnuson A, Rova M, Mamedov F, Fredriksson P-O, Styring S. 1999. The role of cytochrome b_{559} and tyrosine$_D$ in protection against photoinhibition during in vivo photoactivation of photosystem II. *Biochim. Biophys. Acta* 1411:180–91
141. Mamedov F, Styring S. 2003. Logistics in the life cycle of photosystem II—lateral movement in the thylakoid membrane and activation of electron transfer. *Physiol. Plant.* 119:328–36
142. Faller P, Debus RJ, Brettel K, Sugiura M, Rutherford AW, Boussac A. 2001. Rapid formation of the stable tyrosyl radical in photosystem II. *Proc. Natl. Acad. Sci. USA* 98:14368–73
143. Ananyev GM, Sakiyan I, Diner BA, Dismukes GC. 2001. A functional role for tyrosine-D in assembly of the inorganic core of the water oxidase complex of photosystem II and the kinetics of water oxidation. *Biochemistry* 41:974–80
144. Tracewell CA, Cua A, Stewart DH, Bocian DF, Brudvig GW. 2000. Characterization of carotenoid and chlorophyll photooxidation in photosystem II. *Biochemistry* 40:193–203
145. Falkowski PG, Fujita Y, Ley A, Mauzerall D. 1986. Evidence for cyclic electron flow around photosystem II in *Chlorella pyrenoidosa*. *Plant Physiol.* 81:310–12
146. Prasil O, Kolber Z, Berry JA, Falkowski PG. 1996. Cyclic electron flow around photosystem II in vivo. *Photosynth. Res.* 48:395–410
147. Grabolle M, Dau H. 2007. Efficiency and role of loss processes in light-driven water oxidation by PSII. *Physiol. Plant.* 131:50–63
148. Vass I, Cser K. 2009. Janus-faced charge recombinations in photosystem II photoinhibition. *Trends Plant Sci.* 14:200–5
149. Rutherford AW, Osyczka A, Rappaport F. 2012. Back-reactions, short-circuits, leaks and other energy wasteful reactions in biological electron transfer: redox tuning to survive life in O_2. *FEBS Lett.* 586:603–16
150. Reinman S, Mathis P. 1981. Influence of temperature on photosystem II electron transfer reactions. *Biochim. Biophys. Acta* 635:249–58
151. Moser CC, Page CC, Leslie Dutton P. 2005. Tunneling in PSII. *Photochem. Photobiol. Sci.* 4:933–39
152. Vass I, Styring S, Hundal T, Koivuniemi A, Aro E, Andersson B. 1992. Reversible and irreversible intermediates during photoinhibition of photosystem II: stable reduced Q_A species promote chlorophyll triplet formation. *Proc. Natl. Acad. Sci. USA* 89:1408–12
153. Krieger-Liszkay A, Fufezan C, Trebst A. 2008. Singlet oxygen production in photosystem II and related protection mechanism. *Photosynth. Res.* 98:551–64
154. Kruse O, Rupprecht J, Mussgnug JH, Dismukes GC, Hankamer B. 2005. Photosynthesis: a blueprint for solar energy capture and biohydrogen production technologies. *Photochem. Photobiol. Sci.* 4:957–70
155. Rappaport F, Diner BA. 2008. Primary photochemistry and energetics leading to the oxidation of the $(Mn)_4Ca$ cluster and to the evolution of molecular oxygen in photosystem II. *Coord. Chem. Rev.* 252:259–72
156. Moser CC, Dutton PL. 1992. Engineering protein structure for electron transfer function in photosynthetic reaction centers. *Biochim. Biophys. Acta* 1101:171–76

157. Sugiura M, Inoue Y. 1999. Highly purified thermo-stable oxygen-evolving photosystem II core complex from the thermophilic cyanobacterium *Synechococcus elongatus* having His-tagged CP43. *Plant Cell Physiol.* 40:1219–31
158. Kolber ZS, Prasil O, Falkowski PG. 1998. Measurements of variable chlorophyll fluorescence using fast repetition rate techniques: defining methodology and experimental protocols. *Biochim. Biophys. Acta* 1367:88–106
159. Shinkarev VP. 2005. Flash-induced oxygen evolution in photosynthesis: simple solution for the extended S-state model that includes misses, double-hits, inactivation, and backward-transitions. *Biophys. J.* 88:412–21
160. Zheng M, Dismukes GC. 1996. Orbital configurations of the valence electrons, ligand field symmetry and manganese oxidation states of the photosynthetic water oxidizing complex: analysis of the S_2 state multiline EPR signals. *Inorg. Chem.* 35:3307–19
161. Messinger J, Nugent JHA, Evans MCW. 1997. Detection of an EPR multiline signal for the S_0 state in photosystem II. *Biochemistry* 36:11055–60
162. Brynda M, Britt RD. 2010. The manganese-calcium cluster of the oxygen-evolving system: synethic models, EPR studies, and electronic structure calculations. In *Metals in Biology*, ed. G Hanson, L Berliner, pp. 203–55. New York: Springer. 419 pp.
163. Carrell TG, Tyryshkin AM, Dismukes GC. 2002. An evaluation of structural models for the photosynthetic water-oxidizing complex derived from spectroscopic and X-ray diffraction signatures. *J. Biol. Inorg. Chem.* 7:2–22
164. Kuzek D, Pace RJ. 2001. Probing the manganese oxidation states in the oxygen evolving complex: insights from spectroscopic, computational, and kinetic data. *Biochim. Biophys. Acta* 1503:123–37
165. Lubitz W, Reijerse EJ, Messinger J. 2008. Solar water-splitting into H_2 and O_2: design principles of photosystem II and hydrogenases. *Energy Environ. Sci.* 1:15–31
166. Dau H, Haumann M. 2008. The manganese complex of photosystem II in its reaction cycle—basic framework and possible realization at the atomic level. *Coord. Chem. Rev.* 252:273–95
167. Dau H, Liebisch P, Haumann M. 2003. X-ray absorption spectroscopy to analyze nuclear geometry and electronic structure of biological metal centers—potential and questions examined with special focus on the tetra-nuclear manganese complex of oxygenic photosynthesis. *Anal. Bioanal. Chem.* 376:562–83
168. Magnuson A, Liebisch P, Högblom J, Anderlund MF, Lomoth R, et al. 2006. Bridging-type changes facilitate successive oxidation steps at about 1 V in two binuclear manganese complexes—implications for photosynthetic water-oxidation. *J. Inorg. Biochem.* 100:1234–43
169. Messinger J, Robblee JH, Bergmann U, Fernandez C, Glatzel P, et al. 2001. Absence of Mn-centered oxidation in the $S_2 \rightarrow S3$ transition: implications for the mechanism of photosynthetic water oxidation. *J. Am. Chem. Soc.* 123:7804–20
170. Yachandra VK, Sauer K, Klein MP. 1996. Manganese cluster in photosynthesis: where plants oxidize water to dioxygen. *Chem. Rev.* 96:2927–50
171. Bergmann U, Grush MM, Horne CR, DeMarois P, Penner-Hahn JE, et al. 1998. Characterization of the Mn oxidation states in photosystem II by Kβ X-ray fluorescence spectroscopy. *J. Phys. Chem.* 102:8350–52
172. Glatzel P, Bergmann U, Yano J, Visser H, Robblee JH, et al. 2004. The electronic structure of Mn in oxides, coordination complexes, and the oxygen-evolving complex of photosystem II studied by resonant inelastic X-ray scattering. *J. Am. Chem. Soc.* 126:9946–59
173. Pace RJ, Jin L, Stranger R. 2012. What spectroscopy reveals concerning the Mn oxidation levels in the oxygen evolving complex of photosystem II: X-ray to near infra-red. *Dalton Trans.* 41:11145–60
174. Kulik LV, Epel B, Lubitz W, Messinger J. 2005. ^{55}Mn pulse ENDOR at 34 GHz of the S_0 and S_2 states of the oxygen-evolving complex in photosystem II. *J. Am. Chem. Soc.* 127:2392–93
175. Kulik LV, Epel B, Lubitz W, Messinger J. 2007. Electronic structure of the Mn_4O_xCa cluster in the S_0 and S_2 states of the oxygen-evolving complex of photosystem II based on pulse ^{55}Mn-ENDOR and EPR spectroscopy. *J. Am. Chem. Soc.* 129:13421–35
176. Abragam A, Bleaney B. 1970. *Electron Paramagnetic Resonance of Transition Ions*. Oxford, UK: Oxford Univ. Press. 944 pp.

177. Kuntzleman T, Yocum CF. 2005. Reduction-induced inhibition and Mn(II) release from the photosystem II oxygen-evolving complex by hydroquinone or NH_2OH are consistent with a Mn(III)/Mn(III)/Mn(IV)/Mn(IV) oxidation state for the dark-adapted enzyme. *Biochemistry* 44:2129–42
178. Nugent JHA, Muhiuddin IP, Evans MCW. 2003. Effect of hydroxylamine on photosystem II: reinvestigation of electron paramagnetic resonance characteristics reveals possible S state intermediates. *Biochemistry* 42:5500–7
179. Sivaraja M, Dismukes GC. 1988. Binding of hydroxylamine to the water-oxidizing complex and the ferroquinone electron acceptor of spinach photosystem II. *Biochemistry* 27:3467–75
180. Hillier W, Wydrzynski T. 2001. Oxygen ligand exchange at metal sites—implications for the O_2 evolving mechanism of photosystem II. *Biochim. Biophys. Acta* 1503:197–209
181. Babcock GT, Ghanotakis DF, Ke B, Diner BA. 1983. Electron donation to photosystem II in reaction center preparations. *Biochim. Biophys. Acta* 723:276–86
182. Sugiura M, Minagawa J, Inoue Y. 1999. Properties of *Chlamydomonas* photosystem II core complex with a His-tag at the C-terminus of the D2 protein. *Plant Cell Physiol.* 40:311–18
183. Tang X-S, Diner BA. 1994. Biochemical and spectroscopic characterization of a new oxygen-evolving photosystem II core complex from the cyanobacterium *Synechocystis* PCC 6803. *Biochemistry* 33:4594–603
184. Noren GH, Boerner RJ, Barry BA. 1991. EPR characterization of an oxygen-evolving photosystem II preparation from the transformable cyanobacterium *Synechocystis* 6803. *Biochemistry* 30:3943–50
185. Bricker TM, Morvant J, Masri N, Sutton HM, Frankel LK. 1998. Isolation of a highly active photosystem II preparation from *Synechocystis* 6803 using a histidine-tagged mutant of CP47. *Biochim. Biophys. Acta* 1409:50–57
186. Hillier W, Wydrzynski T. 2000. The affinities for the two substrate water binding sites in the O_2 evolving complex of photosystem II vary independently during S-state turnover. *Biochemistry* 39:4399–405
187. Hillier W, Wydrzynski T. 2004. Substrate water interactions within the photosystem II oxygen evolving complex. *Phys. Chem. Chem. Phys.* 6:4882–89
188. Dau H, Sauer K. 1996. Exciton equilibration and photosystem II exciton dynamics—a fluorescence study on photosystem II membrane particles of spinach. *Biochim. Biophys. Acta* 1273:175–90
189. Holzwarth AR, Müller MG, Reus M, Nowaczyk M, Sander J, Rögner M. 2006. Kinetics and mechanism of electron transfer in intact photosystem II and in the isolated reaction center: Pheophytin is the primary electron acceptor. *Proc. Natl. Acad. Sci. USA* 103:6895–900
190. Schatz GH, Brock H, Holzwarth AR. 1988. Kinetic and energetic model for the primary processes in photosystem II. *Biophys. J.* 54:397–405
191. Nuijs AM, Shuvalov VA, van Gorkom HJ, Plijter JJ, Duysens LNM. 1986. Picosecond absorbance difference spectroscopy on the primary reactions and the antenna-excited states in photosystem I particles. *Biochim. Biophys. Acta* 850:310–18
192. Schatz GH, Brock H, Holzwarth AR. 1987. Picosecond kinetics of fluorescence and absorbance changes in photosystem II particles excited at low photon density. *Proc. Natl. Acad. Sci. USA* 84:8414–18
193. Cao J, Govindjee. 1990. Chlorophyll a fluorescence transient as an indicator of active and inactive photosystem II in thylakoid membranes. *Biochim. Biophys. Acta* 1015:180–88
194. Whitmarsh J, Cramer WA. 1977. Kinetics of the photoreduction of cytochrome *b*-559 by photosystem II in chloroplasts. *Biochim. Biophys. Acta* 460:280–89
195. Buser CA, Diner BA, Brudvig GW. 1992. Photooxidation of cytochrome *b*559 in oxygen-evolving photosystem II. *Biochemistry* 31:11449–59
196. Volk M, Gilbert M, Rousseau G, Richter M, Ogrodnik A, Michel-Beyerle M-E. 1993. Similarity of primary radical pair recombination in photosystem II and bacterial reaction centers. *FEBS Lett.* 336:357–62
197. Vos MH, van Gorkom HJ, van Leeuwen PJ. 1991. An electroluminescence study of stabilization reactions in the oxygen-evolving complex of photosystem II. *Biochim. Biophys. Acta* 1056:27–39
198. Rappaport F, Guergova-Kuras M, Nixon PJ, Diner BA, Lavergne J. 2002. Kinetics and pathways of charge recombination in photosystem II. *Biochemistry* 41:8518–27
199. Johnson GN, Rutherford AW, Krieger A. 1995. A change in the midpoint potential of the quinone Q_A in photosystem II associated with photoactivation of oxygen evolution. *Biochim. Biophys. Acta* 1229:202–7

200. Krieger A, Rutherford AW, Johnson GN. 1995. On the determination of redox midpoint potential of the primary quinone electron acceptor, Q_A, in photosystem II. *Biochim. Biophys. Acta* 1229:193–201
201. Grabolle M, Dau H. 2005. Energetics of primary and secondary electron transfer in photosystem II membrane particles of spinach revisited on basis of recombination-fluorescence measurements. *Biochim. Biophys. Acta* 1708:209–18
202. Gorkom HJ. 1985. Electron transfer in photosystem II. *Photosynth. Res.* 6:97–112
203. Minagawa J, Narusaka Y, Inoue Y, Satoh K. 1998. Electron transfer between Q_A and Q_B in photosystem II is thermodynamically perturbed in phototolerant mutants of *Synechocystis* sp. PCC 6803. *Biochemistry* 38:770–75
204. Wydrzynski TJ, Satoh K, eds. 2005. *Photosystem II: The Light-Driven Water:Plastoquinone Oxidoreductases*. Dordrecht, Neth.: Springer. 786 pp.